Supplemental Data

Vascular stiffness mechanoactivates YAP/TAZ-dependent glutaminolysis to drive pulmonary hypertension

Thomas Bertero, William M. Oldham, Katherine A. Cottrill, Sabrina Pisano, Rebecca R. Vanderpool, Qiujun Yu, Jingsi Zhao, Yiyin Tai, Ying Tang, Ying-Yi Zhang, Sofiya Rehman, Masataka Sugahara, Zhi Qi, John Gorcsan III, Sara O. Vargas, Rajan Saggar, Rajeev Saggar, W. Dean Wallace, David J. Ross, Kathleen J. Haley, Aaron B. Waxman, Victoria N. Parikh, Teresa De Marco, Priscilla Y. Hsue, Alison Morris, Marc A. Simon, Karen A. Norris, Cedric Gaggioli, Joseph Loscalzo, Joshua Fessel, and Stephen Y. Chan

Supplemental Figure Legends

Figure S1: ECM stiffening activates glycolysis and glutaminolysis in PASMCs. A) By extracellular flux analysis, PASMCs cultivated in stiff matrix displayed decreased oxygen consumption rate (OCR) and increased extracellular acidification rate (ECAR), reflective of glycolysis. **B)** As assessed by ECAR, PASMCs cultivated in stiff matrix displayed increased basal glycolysis and corresponding decreased glycolytic reserve (as assessed by the difference between oligomycin A-induced ECAR and basal ECAR). **C)** Basal OCR, ATP dependent OCR (difference between basal OCR and oligomycin A-inhibited OCR), and respiratory reserved (maximal FCCP-induced OCR) were decreased in PASMCs in stiff matrix. **D)** Mitotracker labeling confirmed a decrease of mitochondrial activity in PASMCs in stiff matrix. **E)** In PASMCs in stiff matrix, targeted LC-MS/MS revealed an increased lactate/pyruvate ratio, indicative of increased glycolysis. **F)** In these same cells, glutamine, pyruvate, and succinate were decreased, while glutamate and aspartate were increased. **G)** Released lactate was progressively increased in PASMCs cultivated in an increasing gradient of matrix stiffness. **H-J)** In PASMCs, GLS1, LDHA, and PC expression was increased by matrix stiffening, as confirmed by RT-qPCR (CTGF was used as an internal positive control) (**H**), and by immunoblot and densitometry quantification (**I-J**). **K)** In PAECs and PASMCs, expression of the two GLS1 isoforms, KGA and GAC, was increased by matrix stiffening, as confirmed by RT-qPCR. **L)** In PAECs, GLS2 expression was not affected by matrix stiffening, as confirmed by RT-qPCR. In all panels, mean expression in controls (soft matrix) was assigned a fold change of 1, to which relevant samples were compared. Data are expressed as mean ± SEM *P<0.05, **P<0.01, ***P<0.001) of at least 3 independent experiments. Scale bars, 20μm.

Figure S2: A metabolic switch induced by ECM stiffening is coordinated by the mechano-action of YAP/TAZ. A) Immunoblot analysis confirmed the knockdown of YAP and TAZ by 2 independent siRNA sequences in PASMCs. **B)** In PASMCs, YAP/TAZ knockdown blunted the

increase in lactate observed in stiff conditions. **C-D)** Similarly, targeted LC-MS/MS revealed that metabolite alterations in PASMCs in stiff matrix (*i.e.*, decreases of intracellular glutamine, pyruvate, and succinate and increases of glutamate and aspartate) were blunted by YAP/TAZ knockdown (**C**). YAP/TAZ knockdown also blunted the increase in lactate/pyruvate ratio (**D**) induced by stiff matrix. **E-F)** RT-qPCR revealed that increased GLS1, LDHA, and PC expression in PASMCs (**E**) and PAECs (**F**) in stiff matrix was blunted by YAP/TAZ knockdown (**E**) but not by YAP or TAZ knockdown alone (**F**). **G)** Immunoblot analysis confirmed the forced expression of YAP in PASMCs infected with a lentiviral vector containing the YAP coding sequences (pYAP) compared to cells infected with a control vector (pGFP). **H)** Forced expression of YAP increased lactate in PASMCs cultivated on soft matrix. **I)** Mitotracker labeling and quantification confirmed that YAP overexpression decreased mitochondrial activity of PASMCs cultivated on soft matrix. In all panels, mean expression in control groups (Soft matrix) was assigned a fold change of 1, to which relevant samples were compared. Data are expressed as mean ± SD (*P<0.05, **P<0.01, ***P<0.001) of at least 3 independent experiments. Scale bars, 20μm.

Figure S3: Genetic or pharmacologic inhibition of GLS decreases glutaminolysis in order to control proliferation of PASMCs exposed to stiff matrix. A-C) In PASMCs, targeted LC-MS/MS revealed that independent GLS1 knockdown (si-GLS1_1 and si-GLS1_2) blunted the alterations of metabolite expression in stiff matrix – specifically, compared with stiff matrix control (si-NC Stiff), increasing glutamine, pyruvate and succinate, decreasing glutamate and aspartate (**A**), decreasing lactate (**B**), and lactate/pyruvate ratio (**C**). **D-F)** In PASMCs, targeted LC-MS/MS revealed that pharmacologic inhibition of GLS (BPTES or DON) blunted the alterations of metabolite expression in stiff matrix – specifically, compared with stiff matrix control (si-NC Stiff), increasing glutamine, pyruvate and succinate, decreasing glutamate and aspartate (**D**), decreasing lactate (**E**), and lactate/pyruvate ratio (**F**). **G-H)** As revealed by cell counting, GLS1 inhibition by either siRNA (**G**) or pharmacologic inhibitors (**H**) in PASMCs

blunted proliferation in stiff, but not soft, matrix. In all panels, mean expression in control groups (soft matrix) was assigned a fold change of 1, to which relevant samples were compared. Data are expressed as mean ± SD (*P<0.05, **P<0.01, ***P<0.001) of at least 3 independent experiments.

Figure S4: Genetic or pharmacologic inhibition of GLS1 controls PAEC proliferation but not apoptosis. A-B) Transcriptomic analyses and network representation (as derived by Reactome FI tool (25) of the alterations in ECM organization (A) and cell cycle (B) in PAECs after GLS1 knockdown in stiff matrix. Green: down-regulated genes; red: up-regulated genes. **C-E)** PAECs were plated on soft (1 kPa) or stiff (50 kPa) matrix and exposed to indicated treatments. Apoptosis (**C-E**) and proliferation (**D-E**) were quantified 48h after plating. **C)** Enzymatic assay revealed an increase of caspase 3/7 activity 24h after serum depletion in soft matrix and, to a lesser extent, in stiff matrix. No significant changes were observed in the presence of pharmacological inhibitors of GLS1 (BPTES, C968) or after GLS1 knockdown by two independent siRNAs (si-GLS1_1, siGLS1_2) as compared with control treatments (Vehicle control; siRNA scrambled control, siNC). **D-E)** As revealed by immunofluorescent microscopy (**D**) and quantification (**E**), proliferation was increased by matrix stiffening (as reflected by PCNA+ stain) but was decreased by pharmacologic GLS1 inhibition. Apoptosis (as reflected by cleaved caspase-3 staining, CC-3+) was increased by serum starvation in both soft and stiff conditions but was not affected by GLS1 inhibition. In all panels, mean expression in control groups (soft matrix) was assigned a fold change of 1, to which relevant samples were compared. Data are expressed as mean ± SD (*P<0.05, **P<0.01, ***P<0.001) of at least 3 independent experiments.

Figure S5: The production of aspartate and glutamate are crucial for YAP/TAZ-dependent glutaminolytic control of PASMC proliferation in stiff matrix. Cell counting revealed that

either siRNA knockdown of GLS1 (left panel) or YAP/TAZ (right panel) decreased proliferation of PASMCs. Supplementation by glutamate or, to a better extent, aspartate sustained proliferation of PASMCs where GLS1 or YAP/TAZ were inhibited. In all panels, mean expression in control groups (soft matrix) was assigned a fold change of 1, to which relevant samples were compared. Data are expressed as mean ± SD (*P<0.05, **P<0.01, ***P<0.001) of at least 3 independent experiments.

Figure S6: Increase of pulmonary arterial stiffness correlates with increases of periarteriolar fibrillar collagen, GLS1 expression, glutaminolysis, and aspartate production in monocrotaline-exposed PAH rats. Rats were administered 60mg/kg of vehicle (n=6) or monocrotaline (n=6) to induce PAH. **A)** Increased hemodynamic manifestation of PAH was confirmed by invasive assessment of right ventricular systolic pressure (RVSP). **B)** After three weeks, picrosirius red staining confirmed increased periarteriolar collagen deposition (parallel) and fibrillar collagen content (orthogonal) in PAH rats compare with vehicle. **C-F)** In PAH CD31+ pulmonary rat cells (n=6), targeted LC-MS/MS revealed that pyruvate (D) and succinate (F) were decreased, while glutamate (C) and α-ketoglutarate (E) were not significantly modulated as compared with non-PAH CD31+ cells (n=6). **G)** Co-immunofluorescence microscopy and quantification confirmed an increase in GLS in both α-SMA+ and CD31+ cells in diseased rat pulmonary arterioles. **H-I)** Immunoblot analysis (H) and densitometry (I) confirmed the increased of GLS in PAH CD31- rat lung cells. **J-K)** Co-immunofluorescence microscopy and quantification revealed that the increase of periarteriolar fibrillar collagen deposition is accompanied by increased LDHA (**J**) and PC (**K**) expression. Such staining further demonstrated an increase in YAP1/LDHA (**J**) and YAP1/PC (**K**) double-positive cells in diseased pulmonary arterioles. In all panels, mean expression in control groups was assigned a

fold change of 1, to which relevant samples were compared. Data are expressed as mean ± SEM (*P<0.05, **P<0.01, ***P<0.001). Scale bars, 50μm.

Figure S7: Timed analyses of monocrotaline-induced PH in rats revealed early pulmonary arteriolar cell apoptosis followed by increased cell proliferation. A-B) Co-immunofluorescence microscopy revealed an early/early-mid (between D3-D7 post-monocrotaline injection) increase of the proliferation marker, Ki67, in both medial (α-SMA+) and intimal (von Willebrand factor, vWF+) pulmonary vascular compartments. **C-E)** As revealed by caspase 3/7 activity assay of whole lung tissue (**C**) and co-immunofluorescence microscopy stain for cleaved caspase-3 (CC-3) (**D-E**), these changes were preceded by very early (between D0 and D3 post-monocrotaline injection) apoptosis in intimal (vWF+) as well as medial (α-SMA+) pulmonary vascular compartments. Data are expressed as mean ± SEM (*P<0.05, **P<0.01, ***P<0.001). Scale bars, 50μm.

Figure S8: **Timed analyses of monocrotaline-induced PH in rats revealed an early/early-mid increase of pulmonary arteriolar GLS1 expression. A)** Co-immunofluorescence microscopy revealed an early/early-mid (between D3-D7 post-monocrotaline injection) increase of GLS1 expression in both medial (α-SMA+) and intimal (CD31+) pulmonary vascular compartments in monocrotaline-injected rats. The two GLS1 isoforms GAC (**B**) and KGA (**C**) were increased in both medial (α-SMA+) and intimal (CD31+) pulmonary vascular compartments in these rats. Data are expressed as mean ± SEM (*P<0.05, **P<0.01, ***P<0.001). Scale bars, 50μm.

Figure S9: Up-regulation of YAP correlates with increased expression of GLS1, LDHA, PC, and the proliferation marker Ki67 in pulmonary arteriolar cells of human patients suffering from multiple forms of PAH. A-B) Co-immunofluorescence microscopy and quantification revealed increased LDHA (**A**) and PC (**B**) expression in human PAH pulmonary arterioles (n=6). Such staining further demonstrated an increase in YAP1/LDHA (**A**) and YAP1/PC (**B**) double-positive cells in diseased arterioles. **C-D)** Similar to findings in monocrotaline-injected rats, GLS1 isoforms, KGA (**C**) and GAC (**D**), were increased in both medial (α-SMA+) and intimal (CD31+) pulmonary arteriolar compartments in human lungs with PAH. **E)** These changes were accompanied by an increase of proliferating pulmonary vascular cells (Ki67+) in both medial (α-SMA+) and endothelial (vWF+) compartments and a modest reduction of vascular apoptotic cells (cleaved caspase-3, CC-3+). Data are expressed as mean ± SEM (*P<0.05, **P<0.01, ***P<0.001). Scale bars, 50μm.

Figure S10: Up-regulation of YAP correlates with increased expression of GLS1 and the proliferation marker Ki67 in plexiform lesions of human patients suffering from multiple forms of PAH. A) In human plexiform lesions with abundant CD31+ cells, an increase of GLS1 was observed. **B)** Further staining demonstrated an increase in YAP1/GLS double-positive cells. **C)** This was accompanied by increased expression of the proliferation marker Ki67 but with relatively sparse cells expressing the apoptotic marker cleaved caspase-3 (CC-3). Data are expressed as mean ± SEM. Scale bars, 50μm.

Figure S11: Up-regulation of YAP correlates with increased expression of GLS1, LDHA, PC, and the proliferation marker Ki67 in pulmonary arteriolar cells of macaques suffering from PAH due to SIV infection. A) In rhesus macaques infected with SIV, α-SMA staining and quantification of arteriolar muscularization confirmed pulmonary arteriolar remodeling in 13 of

the 22 infected monkeys. **B**) Co-immunofluorescence microscopy and quantification revealed an increase of GLS1 in macaques suffering from PAH due to SIV infection (SIV-PAH) in both medial (α-SMA+) and endothelial (vWF+) vascular compartments. **C-D)**The two GLS1 isoforms KGA (**C**) and GAC (**D**) were increased in macaques suffering from PAH due to SIV infection (SIV-PAH) in both medial (α-SMA+) and endothelial (vWF+) vascular compartments. **E)** These changes were accompanied by an increase of proliferating pulmonary vascular cells (Ki67+) in both medial (α-SMA+) and endothelial (vWF+) compartments. In contrast, apoptotic (CC-3+) cells were relatively sparse in both conditions. **F)** Co-immunofluorescence microscopy and quantification revealed an increase of LDHA in macaques suffering from PAH due to SIV infection (SIV-PAH). Such LDHA expression corresponded with up-regulated YAP expression, as reflected by an increase YAP1/LDHA double-positive cells. **G)** Similarly, co-immunofluorescence microscopy revealed an increase of PC in SIV-PAH diseased arterioles. Such PC expression again corresponded with up-regulated YAP expression, as reflected by an increase YAP1/PC double-positive cells. In all panels, mean expression in control groups was assigned a fold change of 1, to which relevant samples were compared. Data are expressed as median denoted by horizontal line (*P<0.05, **P<0.01, ***P<0.001). Scale bars, 50μm.

Figure S12: Left ventricular function, heart rate, and systemic blood pressure were unchanged in rats administered BAPN or verteporfin. A-C) By echocardiography, left ventricular ejection fraction (**A**), fractional shortening (**B**), and interventricular septal thickness at diastole (IVsd, **C**) were unchanged in rats administered BAPN or verteporfin compared with vehicles (n=3/4 rats/group). **D-E)** As measured by invasive catheterization of the abdominal aorta, systemic heart rate (**D**) and mean arterial pressure (**E**) were unchanged in rats administered BAPN or verteporfin compared with vehicles (n=4-7 rats/group). Of note, a trend

was observed toward decreased mean arterial pressure with BAPN treatment (**Fig.S12E**), consistent with prior reports (1). Data are expressed as mean ± SEM.

Figure S13: Left ventricular function, heart rate, and systemic blood pressure were unchanged in rats administered C968 or CB-839. By echocardiography, left ventricular ejection fraction (**A,F**), fractional shortening (**B,G**), and interventricular septal thickness at diastole (IVsd, **C,H**) were unchanged in rats administered C968 (**A-E**) or CB-839 (**F-J**) compared with vehicle (n=4 rats/group). As measured by invasive catheterization of the abdominal aorta, heart rate (**D,I**) and mean arterial pressure (**E,J**) were unchanged in rats administered C968 or CB-839 compared with vehicle (n=4-5 rats/group). Data are expressed as mean ± SEM.

Figure S14: Pharmacologic inhibition of GLS1 in monocrotaline-injected rats does not affect pulmonary arteriolar cell apoptosis. Following monocrotaline injection, via either a C968 disease prevention (**A**) or a CB-839 disease reversal (**B**) dosing protocol, inhibition of glutaminolysis did not alter apoptosis in either medial (α-SMA+) or intimal (CD31+) pulmonary vascular compartments. Data are expressed as mean ± SEM.

Table S1. Pathway enrichment of PAECs genes differentially expressed in response to GLS knockdown in stiff matrix. Pathway enrichment performed by Reactome FI tool (2) incorporating data from KEGG, Reactome, NCBI, and Biocarta databases.

Pathway	Pathway Size	Overlap Size	pval	FDR	Overlapping Genes (Up)	Overlapping Genes (Down)
NF-kappa B signaling pathway (KEGG)	91	9	<0.0001	2.67E-03	LY96	PTGS2 CXCL2 IL8 CXCL12 BCL2A1 TNFAIP3 DDX58 VCAM1
Extracellular matrix organization (Reactome)	263	16	<0.0001	3.00E-03	ADAM9 ADAM17 NID2	LTBP1 PLOD2 ADAMTS1 LAMC2 FGF2 VCAN FBLN5 TGFB2 SDC4 VCAM1 FBN2 COL8A1 COL5A2
Malaria (KEGG)	49	7	<0.0001	3.00E-03	-	CSF3 THBS2 IL8 SELE TGFB2 CCL2 VCAM1
TNF signaling pathway (KEGG)	110	9	0.0001	9.00E-03	-	PTGS2 VEGFC CXCL1 CXCL2 SELE CXCL10 TNFAIP3 CCL2 VCAM1
Beta5 beta6 beta7 and beta8 integrin cell surface interactions (NCBI)	17	4	0.0002	1.76E-02	-	EDIL3 PLAUR CYR61 VCAM1
NOD-like receptor signaling pathway (KEGG)	57	6	0.0003	2.52E-02	-	CXCL1 CXCL2 IL8 TNFAIP3 CCL2 PYDC1
Interferon alpha/beta signaling (Reactome)	63	6	0.0005	3.57E-02	GBP2	OASL MX2 EGR1 IFIT2 IFIT1
E2F transcription factor network (NCBI)	68	6	0.0007	4.69E-02	-	MYBL2 CCNE1 RBBP8 RRM2 TYMS CDC25A
Cytokine-cytokine receptor interaction (KEGG)	265	12	0.0009	5.17E-02	-	VEGFC CXCL1 CSF3 CXCL2 IL8 TNFSF15 CXCL11 CXCL12 TGFB2 CXCL10 CCL2 TNFSF10
Mitotic G1-G1/S phases (Reactome)	134	8	0.0012	6.55E-02	-	MYBL2 CCNE1 CDC7 RRM2 PSMD10 WEE1 TYMS CDC25A

Pathway	Pathway Size	Overlap Size	pval	FDR	Overlapping Genes (Up)	Overlapping Genes (Down)
ATF-2 transcription factor network (NCBI)	58	5	0.0021	1.11E-01	-	IL8 DUSP5 DUSP1 SELE TGFB2
Cell Cycle Checkpoints (Reactome)	118	7	0.0024	1.07E-01	UBE2D1	MAD2L1 CCNE1 CDC7 PSMD10 WEE1 CDC25A
Validated transcriptional targets of AP1 family members Fra1 and Fra2 (NCBI)	36	4	0.0024	1.15E-01	HMOX1	PLAUR IL8 CCL2
Beta1 integrin cell surface interactions (NCBI)	66	5	0.0037	1.48E-01	-	PLAUR LAMC2 THBS2 VCAM1 COL5A2
Beta3 integrin cell surface interactions (NCBI)	43	4	0.0045	1.68E-01	-	EDIL3 PLAUR CYR61 SDC4
AP-1 transcription factor network (NCBI)	70	5	0.0047	1.63E-01	-	CYR61 IL8 DUSP1 CCL2 EGR1
Alpha9 beta1 integrin signaling events (NCBI)	24	3	0.0062	2.08E-01	-	VEGFC SAT1 VCAM1
Amoebiasis (KEGG)	109	6	0.007	2.22E-01	SERPINB9	LAMC2 CXCL1 IL8 TGFB2 COL5A2
Metabolism of amino acids and derivatives (Reactome)	147	7	0.0079	2.38E-01	ENOPH1 NQO1 GCLM	PSMD10 PHGDH GLS SAT1
BARD1 signaling events (NCBI)	29	3	0.0104	2.86E-01	-	CCNE1 RBBP8 BARD1
Beta2 integrin cell surface interactions (NCBI)	29	3	0.0104	2.86E-01	-	PLAUR CYR61 VCAM1
VEGF and VEGFR signaling network (NCBI)	10	2	0.0106	2.66E-01	PGF	VEGFC
Signaling by VEGF (Reactome)	10	2	0.0106	2.66E-01	PGF	VEGFC
ECM-receptor interaction (KEGG)	86	5	0.0109	2.62E-01	-	LAMC2 THBS2 RELN SDC4 COL5A2

Pathway	Pathway Size	Overlap Size	pval	FDR	Overlapping Genes (Up)	Overlapping Genes (Down)
Cell cycle (KEGG)	124	6	0.0126	2.90E-01	-	MAD2L1 CCNE1 CDC7 TGFB2 WEE1 CDC25A
Rheumatoid arthritis (KEGG)	90	5	0.013	2.87E-01	-	CXCL1 IL8 CXCL12 TGFB2 CCL2
Syndecan-4-mediated signaling events (NCBI)	32	3	0.0135	2.85E-01	-	FGF2 CXCL12 SDC4
ATM pathway (NCBI)	34	3	0.0158	3.20E-01	-	XRCC4 RBBP8 CDC25A
Interferon gamma signaling (Reactome)	63	4	0.0166	3.23E-01	GBP2	OASL GBP1 VCAM1
PI3K-Akt signaling pathway (KEGG)	346	11	0.0181	3.41E-01	PGF PPP2R3A	VEGFC LAMC2 FGF5 CCNE1 FGF2 CSF3 THBS2 RELN COL5A2
ErbB1 downstream signaling (NCBI)	100	5	0.0195	3.57E-01	F2RL2	ZFP36 DUSP1 DIAPH3 EGR1
Extrinsic Pathway for Apoptosis (Reactome)	14	2	0.0199	3.53E-01	ADAM17	TNFSF10
p53 signaling pathway (KEGG)	68	4	0.0212	3.66E-01	ZMAT3	CCNE1 RRM2 PMAIP1
Pyrimidine metabolism (KEGG)	105	5	0.0235	3.91E-01	TK2	CDA RRM2 PNPT1 TYMS
Cell adhesion molecules (CAMs) (KEGG)	143	6	0.0236	3.81E-01	-	VCAN SELE CD274 SDC4 CDH2 VCAM1
ISG15 antiviral mechanism (Reactome)	71	4	0.0244	3.82E-01	-	HERC5 MX2 DDX58 IFIT1
Chemokine signaling pathway (KEGG)	189	7	0.0272	4.10E-01	-	CXCL1 CXCL2 IL8 CXCL11 CXCL12 CXCL10 CCL2
RIG-I/MDA5 mediated induction of IFN-alpha/beta pathways (Reactome)	79	4	0.0341	4.87E-01	UBE2D1	HERC5 TNFAIP3 DDX58

Pathway	Pathway Size	Overlap Size	pval	FDR	Overlapping Genes (Up)	Overlapping Genes (Down)
Calcineurin-regulated NFAT-dependent transcription in lymphocytes (NCBI)	46	3	0.0344	4.66E-01	-	PTGS2 IL8 EGR1
FGF signaling pathway (NCBI)	46	3	0.0344	4.66E-01	-	PLAUR SPRY2 CDH2
Sprouty regulation of tyrosine kinase signals (Biocarta)	19	2	0.0349	4.50E-01	-	SPRY4 SPRY2
Cholesterol biosynthesis (Reactome)	19	2	0.0349	4.50E-01	HMGCS1 DHCR24	-
GPCR ligand binding (Reactome)	433	12	0.0351	4.42E-01	F2RL2	HTR1B CXCL1 CXCL2 IL8 CXCL11 CXCL12 CXCL10 CCL2 P2RY1 PTGER4 ADRB2
TGF-beta signaling pathway (KEGG)	80	4	0.0354	4.34E-01	-	LTBP1 GDF6 FST TGFB2
Segmentation clock (Biocarta)	21	2	0.0418	4.95E-01	ADAM17	DKK2
Inhibition of matrix metalloproteinases (Biocarta)	3	1	0.0449	5.25E-01	-	RECK
Double-Strand Break Repair (Reactome)	22	2	0.0454	5.20E-01	-	XRCC4 BRIP1
Axon guidance (KEGG)	127	5	0.0468	5.30E-01	-	SEMA6D SEMA3C SEMA3A SLIT2 CXCL12
Signaling by EGFR (Reactome)	171	6	0.049	5.48E-01	ADAM17 TNRC6A	FGF5 FGF2 ITPR2 SPRY2
Signaling events mediated by PRL (NCBI)	23	2	0.0491	5.38E-01	-	CCNE1 EGR1

Table S2. Clinical characteristics of PAH patients used for in situ staining.

Age	Gender	mPAP (mmHg)	Clinical description
34	Female	50	Cardiopulmonary arrest (autopsy), Idiopathic
64	Female	55	Cardiopulmonary arrest (autopsy), Idiopathic
68	Female	44	Bilateral lung transplant, Scleroderma
12	Male	53	Bilateral lung transplant, BMPRII mutation
16	Male	62	Bilateral lung transplant, Idiopathic
1	Male	50	Lung resection, Trisomy 21
19	Male	48	Lung resection, Idiopathic
51	Male	48	Lung transplant, Scleroderma
42	Female	57	Lung transplant, Scleroderma
67	Male	50	Lung transplant, Scleroderma
60	Female	66	Autopsy Scleroderma
54	Female	54	Autopsy Scleroderma
72	Female	53	Autopsy Scleroderma

Table S3. Clinical characteristics of PH patients from whom plasma was drawn for metabolite profiling from the main pulmonary artery during pulmonary arterial catheterization. Mean pulmonary arterial pressure (mPAP), pulmonary vascular resistance (PVR).

Age (Year)	Gender	mPAP (mmHg)	PVR (dynes.sec.cm^{-5})
73	Female	37	481
88	Female	46	631
65	Female	49	789
44	Female	46	387
67	Female	45	607
83	Male	54	926
81	Female	52	1031
52	Male	56	522
78	Female	51	960
67	Female	49	560
88	Female	45	542
56	Male	56	1396
67	Female	57	658
81	Female	42	663
23	Male	40	957
78	Female	44	536
79	Female	56	897
80	Male	50	826
78	Male	43	803

Table S4. Clinical characteristics of HIV-infected individuals analyzed for pulmonary arterial compliance by invasive pulmonary arterial catheterization. Ejection fraction (EF); interquartile range (IQR); mean pulmonary artery pressure (mPAP); pulmonary arterial hypertension (PAH); pulmonary capillary wedge pressure (PCWP); pulmonary vascular resistance (PVR)

Variable	**No PAH (n=31)**	**PAH (n=11)**	p-value
Age, median (IQR)	54 (46, 61)	45 (41, 54)	0.14
Age, mean ± SD	53 ± 11	47 ± 9	0.11
Males, n (%)	25 (80.6)	7 (63.6)	0.25
Caucasian, n (%)	19 (61.3)	5 (45.5)	0.36
African-American, n (%)	12 (38.7)	6 (54.5)	
Ever smoker, n (%)	16 (55.2)	7 (77.8)	0.23
Systemic hypertension, n (%)	14 (48.3)	1 (11.1)	**0.046**
Coronary artery disease, n (%)	7 (23.3)	0 (0.0)	0.11
Hepatic disease, n (%)	8 (26.7)	2 (20.0)	0.673
COPD, n (%)	5 (16.7)	1 (11.1)	0.685
mPAP mmHg, median (IQR)	20 (17, 30)	37 (31, 52)	**<0.001**
PCWP mmHg, median (IQR)	13 (9, 21)	11 (7, 13)	0.2
PVR woods unit, median (IQR)	1.4 (1, 1.9)	3.9 (3.5, 10.8)	**<0.001**
PVR≥ 3 woods unit, n (%)	3 (12)	10 (91)	**<0.001**
EF≤45%, n (%)	4 (13.3)	1 (9)	0.71
Diastolic Dysfunction, n (%)	7 (26)	2 (20)	0.7

Table S5. Hemodynamic measurements of HIV-infected individuals with PAH from whom peripheral venous plasma was drawn for metabolite profiling. Mean pulmonary artery pressure (mPAP, as measured by invasive hemodynamics); pulmonary arterial systolic pressure (PASP, as estimated by echocardiography.

Age (Year)	mPAP (mmHg)	PASP (mmHg)
44	35	81
37	37	63
36	38	74
60	47	60
35	51	67
37	53	84
48	55	73
45	56	73
41	58	71

Supplemental Experimental Procedures

Cell Culture and Reagents

HEK293T cells (American Type Culture Collection) were cultivated in DMEM containing 10% fetal bovine serum (FBS). Primary human pulmonary arterial endothelial cells (PAECs) were grown in EGM-2 cell culture media (Lonza), and experiments were performed at passages 3 to 6. Primary human pulmonary arterial smooth muscle cells (PASMCs) were cultured in SmGM-2 cell culture media (Lonza), and experiments were performed at passages 3 to 9. Inhibitors of GLS1 (3, 4): BPTES (Bis-2-(5-phenylacetamido-1,3,4-thiadiazol-2-yl)ethyl sulphide), DON (6-Diazo-5-oxo-L-norleucine), and C968 (Glutaminase Inhibitor, Compound 968, 5-(3-Bromo-4-(dimethylamino)phenyl)-2,2-dimethyl-2,3,5,6-tetrahydrobenzo[a]phenanthridin-4(1H)-one) were purchased from Sigma-Aldrich and used at concentration of 10μM, 5μM and 10μM respectively. Glutamate was purchased from Sigma Aldrich and used at concentration of 2mM; aspartate was purchased from Sigma Aldrich and used at concentration of 10mM, consistent with prior in vitro studies linking cancer cell proliferation to glutamine metabolism and aspartate levels (5, 6).

Oligonucleotides and Transfection

On Target Plus siRNAs for YAP (J-012200-07 and J-012200-05,), TAZ (WWTR1; J-016083-05 and J-016083-06), GLS1 (J-004548-09, si-GLS1_1; J-004548-10, si-GLS1_2), and scrambled control D-001810-01 and D-001810-02) were purchased from ThermoScientific/Dharmacon. siRNA experiments are representative of results obtain with either siYAP_1/TAZ_1 or siYAP_2/TAZ_2. PAECs, and PASMCs were plated in collagen-coated plastic (50μg/mL) and transfected 24h later at 70-80% confluence using siRNA (25nM) and Lipofectamine 2000 reagent (Thermo Fisher Scientific), according to the manufacturers' instructions. Eight hours after transfection, cells were trypsinized and re-plated on hydrogel.

Plasmids

The YAP1 coding sequence was purchased (Addgene; Plasmid #18881) and sub-cloned in the pCDH-CMV-MCS-EF1-copGFP (System Biosciences) using EcoRI and NotI restriction sites. The lentiviral parent vector expressing GFP was used as a control. Stable expression of these constructs in PAECs, and PASMCs was achieved by lentiviral transduction. All cloned plasmids were confirmed by DNA sequencing.

Lentivirus production

HEK293T cells were transfected using Lipofectamine 2000 (Thermo Fisher Scientific) with lentiviral plasmids along with packaging plasmids (pPACK, System Biosciences), according to the manufacturer's instructions. Virus was harvested, sterile filtered (0.45 μm), and utilized for subsequent infection of PAECs, and PASMCs (24-48 hours incubation) for gene transduction.

Messenger RNA extraction

Cells were homogenized in 1 ml of QiaZol reagent (Qiagen). Total RNA content, was extracted using the miRNeasy kit (Qiagen) according to the manufacturer's instructions. Total RNA concentration was determined using a ND-1000 micro-spectrophotometer (NanoDrop Technologies).

Quantitative RT-PCR of messenger RNAs

Messenger RNAs were reverse transcribed using the Multiscript RT kit (Thermo Fisher Scientific) to generate cDNA. cDNA for specific gene targets was amplified and quantified via inventoried fluorescently labeled Taqman primer sets (Thermo Fisher Scientific) using an Applied Biosystems 7900HT Fast Real Time PCR device. To distinguish the relative expression of the two GLS1 isoforms KGA and GAC, TaqMan gene expression assays Hs01014019_m1

and Hs01022166_m1 were used respectively. Fold-change of RNA species was calculated using the formula ($2^{-\Delta\Delta Ct}$), normalized to RPLP0 expression.

ChIP-qPCR

PAECs were cultivated on plastic for 48h. Cells were dual cross-linked with 2 mM disuccinimidyl glutarate (DSG) for 45 minutes and then in 1% paraformaldehyde for 15 minutes at room temperature. Fixed cells were lysed in 10 ml of Lysis Buffer 1 [50 mM HEPES (pH 7.5), 140 mM NaCl, 1 mM EDTA, 0.1% IGEPAL 630 (Sigma Aldrich)], containing 0.05% Triton X100, 2.5 % glycerol and supplemented with 1X protease inhibitor cocktail (Roche) for 10 minutes on ice, followed by incubation in Buffer 2 [0.1 M Tris HCl (pH 8) and 200 mM NaCl with protease inhibitors] for 15 minutes at room temperature. Chromatin was sonicated at 30% of amplitude for 10 minutes (10 cycles of 1 minute). The samples were centrifuged (2X 14,000 g for 5 minutes each), and soluble chromatin was transferred to a fresh tube. Crosslinked DNA after sonication was precipitated with 5µg of anti-YAP1 antibody (sc-15407X, Santa Cruz Biotechnology) or non-immune rabbit IgG (ab27472, Abcam) overnight at 4°C. Chromatin/antibody complex was pulled down with PureProteome™ Protein G Magnetic Beads (Millipore) and washed in the low- and high-salt buffers. After crosslinking reversion (65°C for 4 hours) and Proteinase K treatment, chromatin was purified by phenol-chloroform extraction and ethanol precipitation. Precipitated DNA was analyzed by qPCR using primers generated for predicted TEAD binding sites or a non-relevant genomic region (Control).

Microarrays

PAECs were transfected with a siRNA control (si-NC) or a siRNA against GLS (si-GLS_1) and cultivated on soft hydrogel (1kPa) or stiff hydrogel (50kPa). Forty-eight hours post-transfection, cells were lysed, and RNA was extracted for hybridization on Affymetrix microarrays (HuGene 2.0 ST), according to the manufacturer's instruction. Briefly, total RNA was extracted from

PAECs cells using the miRNeasy kit (Qiagen) according to the manufacturer's instructions. Total RNA concentration was determined using an ND-1000 micro-spectrophotometer (NanoDrop Technologies). Biotinylated cDNA were prepared from 100ng of total RNA using the WT Plus amplification kit (Affymetrix). Following fragmentation, 5.5μg of cDNA were hybridized to the GeneChip Human Gene 2.0 ST Array (Affymetrix). GeneChips were washed and stained in the Affymetrix Fluidics Station 450 and scanned using the Affymetrix GeneChip Scanner 3000 7G. Raw data were normalized using RMA in the Affymetrix Expression Console and presented as log transformed signal intensity.

Pathway Enrichment Analysis

A one-way ANOVA test was used on a gene-by-gene basis to test for differential expression between si-GLS-treated and vehicle-treated PAECs on both soft and stiff matrix backgrounds. Differentially expressed genes were selected based on a p-value cutoff of 0.05 and a fold-change cutoff of 1.5. Pathway enrichment of differentially expressed genes was performed using the Reactome FI analysis tool in the Cytoscape 2.8.1 environment (7). Pathway-by-pathway heat maps were generated using the TM4 MultiExperiment Viewer (8).

Immunoblotting and antibodies

Cells were lysed in Laemmeli buffer (Boston BioProducts). Protein lysate were resolved by SDS-PAGE and transferred onto a PVDF membrane (Biorad). Membranes were blocked in 5% non-fat milk in TN buffer (50 mM Tris-HCl pH 7.4, 150 mM NaCl) or 5% BSA in TN buffer and incubated in the presence of the primary and then secondary antibodies. After washing in TN buffer containing 0.1% Tween, immunoreactive bands were visualized with the ECL system (Amersham Biosciences). Primary antibody to detect YAP1 (#4912; 1/1000) and primary antibody to detect both YAP and TAZ (#8418; 1/1000) were obtained from Cell Signaling. A primary antibody for TAZ (sc-48805) was obtained from Santa Cruz Biotechnology. Primary

antibodies for GLS1 (ab156876; 1/1000), PC (ab115579; 1/1000), LDHA (ab47010; 1/1000) were obtained from Abcam. Primary antibodies for tubulin (T4026; 1/5000) and for actin (A2066; 1/2000) were obtained from Sigma Aldrich. Appropriate secondary antibodies (anti-rabbit, anti-mouse and anti-goat) coupled to HRP were used (Dako).

Immunofluorescence

After the various indicated treatments, cultured cells were fixed with PBS/PFA 4% for 10 min and permeabilized with PBS/Triton 100X 0.1% for 10min. The cells were then incubated with anti-PCNA (#4912; 1/100; Invitrogen), anti-Ki67 (ab15580; 1/200; Abcam), and/or anti-cleaved caspase-3 (#9661; 1/200; Cell Signaling) at room temperature for 2 hours. Secondary antibodies coupled with Alexa-594 and/or Alexa-488 (A-21207 and A-21202 respectively; Thermo Scientific) were used at 1/500. Nuclei were counterstained with DAPI (Sigma).

Cell counting assays

After specified pre-treatment or transfection protocols as indicated, PAECs or PASMCs were plated in triplicate in 6 well plates at 30 000 cells per well. After overnight incubation for cells to adhere, 6 wells were counted to determine initial count at time of treatments (glutamate, aspartate, BPTES, DON, or C968). After 2 days, 4 days or 6 days, the contents of the wells were trypsinized and counted, and proliferation rate was calculated.

BrdU proliferation assay

Exponentially growing cells were plated in the indicated matrix for 48 hours. For proliferation assays, 5-bromo-2-uridine (BrdU) was added to the cell culture medium for 1 hour, and BrdU incorporated into the DNA was revealed using a detection kit (BrdU Cell Proliferation Assay Kit #6813, Cell Signaling).

Scratch assay

Confluent PAECs were wounded using pipet tips and wound bed closures were followed serially over 10 hours. Brightfield images were taken each hour through a 106 phase contrast objective with a CoolSNAPHQ CCD Camera managed by Metamorph Software (Roper Scientific). Wound bed areas were quantified using the NIH ImageJ sotware (http://rsb.info.nih.gov/ij/).

Mitochondrial potential measurements

As described previously (9), cells were stained with 2nM TMRM (tetramethylrhodamine methyl ester, Thermo Fisher Scientific) and Hoechst (0.1μg/ml) for 30 min at 37°C. 5 to 8 random images per well were recorded using a Nikon TE2000 epifluorescent microscope. Mean cell fluorescence intensity for each image was determined using the NIH ImageJ sotware.

Caspase 3/7 assay

Caspase 3/7 activity was quantified using the Caspase-Glo 3/7 Assay (Promega), according to manufacturer's instructions. Briefly, cells were plated on hydrogel of different stiffness and treated as described. Twenty four hours after plating, cells were cultured in the presence or absence of serum for twenty-four hours. Cells were then lysed and 10μg of total protein were incubated for 1h with the caspase substrates, and luminescence was quantified by plate reader (SynergyHTX multi-mode reader, Biotek). Alternatively, flash frozen rat lung tissue (0.1g/sample) was homogenized in 1mL of assay buffer on ice and centrifuged at 8000g 4°C for 10 min. Protein concentration was determined by Bradford assay. Samples, normalized to total protein (10μg), were assessed for caspase 3/7 activity as above.

Animals

Monocrotaline-treated rats: As we previously described (10, 11), male Sprague-Dawley rats (10-14 week old, Charles River) were injected with 60 mg/kg monocrotaline at time 0; at 0-4 weeks

post-exposure, right heart catheterization was performed followed by harvest of lung tissue for RNA extraction or paraffin embedding, as described below (section: **Tissue harvest**). Prior to tissue harvest, mean arterial pressure and heart rate were measured via 1.4F Millar Mikro-Tip single pressure catheter after direct puncture of the abdominal aorta.

Simian immunodeficiency virus-infected rhesus macaques: As previously described (12), rhesus (RM) macaques, aged 6 to 10 years, were obtained from national primate centers or vendors approved by the Division of Laboratory Animal Research at the University of Pittsburgh. Macaques were intravenously inoculated with SIV ΔB670 (gift of M. Murphey-Corb, University of Pittsburgh). Plasma viral loads and peripheral blood $CD4^+$ T cells were determined by quantitative RT-PCR and flow cytometry. Pulmonary artery catheterization was performed before infection and repeated at 6 months and 10-12 months after infection. Furthermore, lung tissue was obtained during necropsy, and pulmonary arteries were examined by a veterinary pathologist blinded to the identity of the monkeys.

Metabolite extraction from plasma

Accordingly to a previously published protocol (13), metabolites were extracted from 20µL of plasma by adding 80µL cold methanol 100% in which an internal standard (ISTD) was added.

Rodent echocardiography

Echocardiography was performed using a 15-45MHz transthoracic transducer and a VisualSonics Vevo770 system (Fujifilm). Inhaled isoflurane anesthesia was used at 2% in 100% O2 during positioning and hair removal and then decreased to isoflurane 0.8% during imaging. Digital echocardiograms were analyzed off-line for quantitative analysis as previously described (11).

Isolation of rat pulmonary vascular endothelial cells

As previously reported (11, 14), lobes of lung tissue from a rat were diced with scissors, to which 200µL of collagenase D solution (Sigma) was added for a final concentration of 2 mg/ml collagenase D in 4.8 mL HEPES buffer (pH=7.4). After incubation for 30 min at 37°C with automated rotation, 20µL of DNase I (Sigma, final concentration of 80 U/mL DNase I) was added and incubated on ice for 30 min. The solution was filtered twice by a 70 µm cell strainer (BD Biosciences) to yield a single cell suspension. After two rounds of PBS wash, cell pelleting, and resuspension, the ACK lysing buffer (Gibco) was used to remove erythrocytes. Remained cells were incubated 30 min at 4°C with a mouse anti-rat-CD31 antibody (BD Pharmigen 555025). Cells were PBS washed twice and incubated 15 min with anti-mouse IgG1 MicroBeads (Miltenyi Biotec) according to the manufacturer protocol. Single CD31-positive cells were then collected using an autoMACS Pro Separator, per the manufacturer's instructions (Miltenyi Biotec). The purity (>95%) of CD31 positive cells was confirmed by flow cytometric analysis by a FACScan flow cytometer (BD Biosciences) after cells labeling with the FITC-conjugated anti-CD31 (ab33858, Abcam).

Tissue harvest of rat lungs

After physiological measurements, by direct right ventricular puncture, the pulmonary vessels were gently flushed with 1 cc of saline to remove the majority of blood cells, prior to harvesting cardiopulmonary tissue. The heart was removed, followed by dissection and weighing of the right ventricle (RV) and of the left ventricle + septum (LV+S). Organs were then harvested for histological preparation or flash frozen in liquid N2 for subsequent homogenization and extraction of RNA and/or protein. To further process lung tissue specifically, prior to excision, lungs were flushed with PBS at constant low pressure (~10mmHg) via right ventricular cannulation, followed by tracheal inflation of the left lung with 10% neutral-buffered formalin (Sigma-Aldrich) at a pressure of ~20cm H2O. After excision and 16 hours of fixation in 10% neutral-buffered formalin at 25^{O}C, lung tissues were paraffin embedded via an ethanol-xylene

dehydration series, before being sliced into 5µm sections (Hypercenter XP System and Embedding Center, Shandon).

Glutaminase activity assay

According to the manufacturer instructions (Glutaminase Microplate Assay Kit, Cohesion Biosciences), flash frozen rat lung tissue (0.1g/sample) was homogenized in 1mL of assay buffer on ice and centrifuged at 8000g 4°C for 10 min. Protein concentration was determined by Bradford assay. Samples, normalized to total protein (100µg), were incubated with kit reagents for 1 hr at 37°C, and absorbances were measured at 420nm.

Lox activity assay

Lox activity was measured using the Lysyl Oxidase Activity Assay Kit (Ab112139), following the manufacturer instructions and as we previously described (10). Briefly, 5µg of total protein extracts from whole lung, as described above, were analyzed. Extracts were incubated for 30min in presence of 50uL of reaction mixture +/- 500µM BAPN. Fluorescence was monitored with a fluorescence plate reader at Ex/Em = 540/590 nm and fluorescence (a measure of LOX activity) was plotted, where 0 = sample + 500 µM BAPN (complete LOX inhibition).

Immunohistochemistry and immunofluorescence of lung sections

Lung sections (5µm) were deparaffinized and high temperature antigen retrieval was performed, followed by blocking in TBS/BSA 5%, 10% donkey serum and exposure to primary antibody and biotinylated secondary antibody (Vectastain ABC kit, Vector Labs) for immunohistochemistry or Alexa 488, 568 and 647-conjugated secondary antibodies (Thermo Fisher Scientific) for immunofluorescence. A primary antibody against YAP1 (#4912; 1/200 or sc101199; 1/50) were obtained from Cell Signaling and Santa Cruz Biotechnology respectively. Primary antibodies against, GLS1 (ab156876; 1/100), PC (ab115579; 1/100), LDHA (ab47010; 1/200), Ki67

(ab15580; 1/200), vWF (ab6994; 1/200) and α-SMA (ab32575; 1/1000 and ab21027; 1/300) were purchased from Abcam. Specific primary antibodies for the GLS1 isoform KGA (20170-1-AP; 1/100) and the GLS1 isoform GAC (19958-1-AP; 1/100) were purchased from Proteintech. A primary antibody against α-SMA (A2547; 1/300) was purchased from Sigma. A primary antibody against CD31 (sc-1506; 1/100), was purchased from Santa Cruz Biotechnology. A primary antibody against PCNA (13-3900, 1/100) was purchased from Thermo Fisher Scientific. In most cases, color development was achieved by adding streptavidin-biotinylated alkaline phosphatase complex (Vector Labs) followed by Vector Red alkaline phosphatase substrate solution (Vector Labs). Levamisole was added to block endogenous alkaline phosphatase activity (Vector Labs). Pictures were obtained using an Olympus Bx51 microscope or ZEISS LSM Exciter confocal microscope. Small pulmonary vessels (<100 μm diameter) present in a given tissue section (>10 vessels/section) that were not associated with bronchial airways were selected for analysis (N>5 animals/group). Intensity of staining was quantified using ImageJ software (NIH). Vessel thickness was calculated as we previously described (11). Degree of pulmonary arteriolar muscularization was assessed in paraffin-embedded lung sections stained for α–SMA by calculation of the proportion of fully and partially muscularized peripheral (<100 μm diameter) pulmonary arterioles to total peripheral pulmonary arterioles, as previously described (15). All measurements were performed blinded to condition.

Atomic force microscopy

Rat lungs were inflated with 0.025g of OCT by g of body weight, frozen on liquid nitrogen vapor and store at -80°C. Rat lung slices (10 μm thickness) were cut out from their glass slide and the fragment of glass containing the sample was glued on the bottom of a 50 mm dish (Willco Glass Bottom Dish). Before measurements the sample was first rinsed and after covered with 4 ml of PBS 1x. The mechanical properties of the samples were studied using a BioScope Catalyst

atomic force microscope (Bruker) coupled with and optical microscope (Leica DMI6000B) that enables, by phase contrast, to pinpoint the areas of interest. For each sample, 5-9 vessels per rat (< 100 μm diameter) were analyzed using the "Point and Shoot" method, collecting from 35 to 80 force-distance curves at just as many discrete points. The experiments of microindentation were performed in PBS using a probe with a Borosilicate Glass spherical tip (5 μm of diameter) and a cantilever with a nominal spring constant of 0.06 N/m (Novascan). Indentations were carried out using a velocity of 2 μm/s, in relative trigger mode and by setting the trigger threshold to 2 nN. The apparent Young's (elastic) modulus was calculated using the NanoScope Analysis 1.50 software (Bruker), fitting the force curves to the Hertz spherical indentation model and using a Poisson's ratio of 0.4. To avoid large indentation, a minimum and a maximum Force Fit Boundary of 5% and 25% respectively of the whole force curve was taken into account for the fit.

Picrosirius red stain and quantification

Picrosirius red stain was achieved through the use of 5μm paraffin sections stained with 0.1% Picrosirius red (Direct Red80, Sigma-Aldrich) and counterstained with Weigert's hematoxylin to reveal fibrillar collagen. The sections were then serially imaged using with an analyzer and polarizer oriented parallel and orthogonal to each other. Microscope conditions (lamp brightness, condenser opening, objective, zoom, exposure time, and gain parameters) were maintained throughout the imaging of all samples. A minimal threshold was set on appropriate control sections for each experiment in which only the light passing through the orthogonally-oriented polarizers representing fibrous structures (*i.e.*, excluding residual light from the black background) was included. The threshold was maintained for all images across all conditions within each experiment. The area of the transferred regions that was covered by the thresholded light was calculated and at least 10 sections/vessel per condition were averaged together (NIH ImageJ software).

Supplemental References

1. Iwatsuki K, Cardinale GJ, Spector S, and Udenfriend S. Reduction of blood pressure and vascular collagen in hypertensive rats by beta-aminopropionitrile. *Proc Natl Acad Sci U S A.* 1977;74(1):360-2.
2. Croft D, Mundo AF, Haw R, Milacic M, Weiser J, Wu G, Caudy M, Garapati P, Gillespie M, Kamdar MR, et al. The Reactome pathway knowledgebase. *Nucleic Acids Res.* 2014;42(Database issue):D472-7.
3. Wang JB, Erickson JW, Fuji R, Ramachandran S, Gao P, Dinavahi R, Wilson KF, Ambrosio AL, Dias SM, Dang CV, et al. Targeting mitochondrial glutaminase activity inhibits oncogenic transformation. *Cancer Cell.* 2010;18(3):207-19.
4. Hensley CT, Wasti AT, and DeBerardinis RJ. Glutamine and cancer: cell biology, physiology, and clinical opportunities. *J Clin Invest.* 2013;123(9):3678-84.
5. Sullivan LB, Gui DY, Hosios AM, Bush LN, Freinkman E, and Vander Heiden MG. Supporting Aspartate Biosynthesis Is an Essential Function of Respiration in Proliferating Cells. *Cell.* 2015;162(3):552-63.
6. Birsoy K, Wang T, Chen WW, Freinkman E, Abu-Remaileh M, and Sabatini DM. An Essential Role of the Mitochondrial Electron Transport Chain in Cell Proliferation Is to Enable Aspartate Synthesis. *Cell.* 2015;162(3):540-51.
7. Shannon P, Markiel A, Ozier O, Baliga NS, Wang JT, Ramage D, Amin N, Schwikowski B, and Ideker T. Cytoscape: a software environment for integrated models of biomolecular interaction networks. *Genome Res.* 2003;13(11):2498-504.
8. Saeed AI, Sharov V, White J, Li J, Liang W, Bhagabati N, Braisted J, Klapa M, Currier T, Thiagarajan M, et al. TM4: a free, open-source system for microarray data management and analysis. *BioTechniques.* 2003;34(2):374-8.
9. Oldham WM, Clish CB, Yang Y, and Loscalzo J. Hypoxia-Mediated Increases in L-2-hydroxyglutarate Coordinate the Metabolic Response to Reductive Stress. *Cell Metab.* 2015;22(2):291-303.
10. Bertero T, Cotrill KA, Lu Y, Haeger CM, Dieffenbach P, Annis S, Hale A, Bhat B, Kaimal V, Zhang YY, et al. Matrix remodeling promotes pulmonary hypertension through feedback mechanoactivation of the YAP/TAZ-miR-130/301 circuit *Cell Rep.* 2015;13(5):1016-32.
11. Bertero T, Lu Y, Annis S, Hale A, Bhat B, Saggar R, Saggar R, Wallace WD, Ross DJ, Vargas SO, et al. Systems-level regulation of microRNA networks by miR-130/301 promotes pulmonary hypertension. *J Clin Invest.* 2014;124(8):3514-28.
12. George MP, Champion HC, Simon M, Guyach S, Tarantelli R, Kling HM, Brower A, Janssen C, Murphy J, Carney JP, et al. Physiologic changes in a nonhuman primate model of HIV-associated pulmonary arterial hypertension. *Am J Respir Cell Mol Biol.* 2013;48(3):374-81.
13. Yuan M, Breitkopf SB, Yang X, and Asara JM. A positive/negative ion-switching, targeted mass spectrometry-based metabolomics platform for bodily fluids, cells, and fresh and fixed tissue. *Nat Protoc.* 2012;7(5):872-81.
14. White K, Lu Y, Annis S, Hale AE, Chau BN, Dahlman JE, Hemann C, Opotowsky AR, Vargas SO, Rosas I, et al. Genetic and hypoxic alterations of the microRNA-210-ISCU1/2 axis promote iron-sulfur deficiency and pulmonary hypertension. *EMBO Mol Med.* 2015;7(6):695-713.
15. Hansmann G, Wagner R, Schellong S, Perez V, Urashima T, Wang L, Sheikh A, Suen R, Stewart D, and Rabinovitch M. Pulmonary arterial hypertension is linked to insulin resistance and reversed by peroxisome proliferator-activated receptor-gamma activation. *Circulation.* 2007;115(10):1275-84.

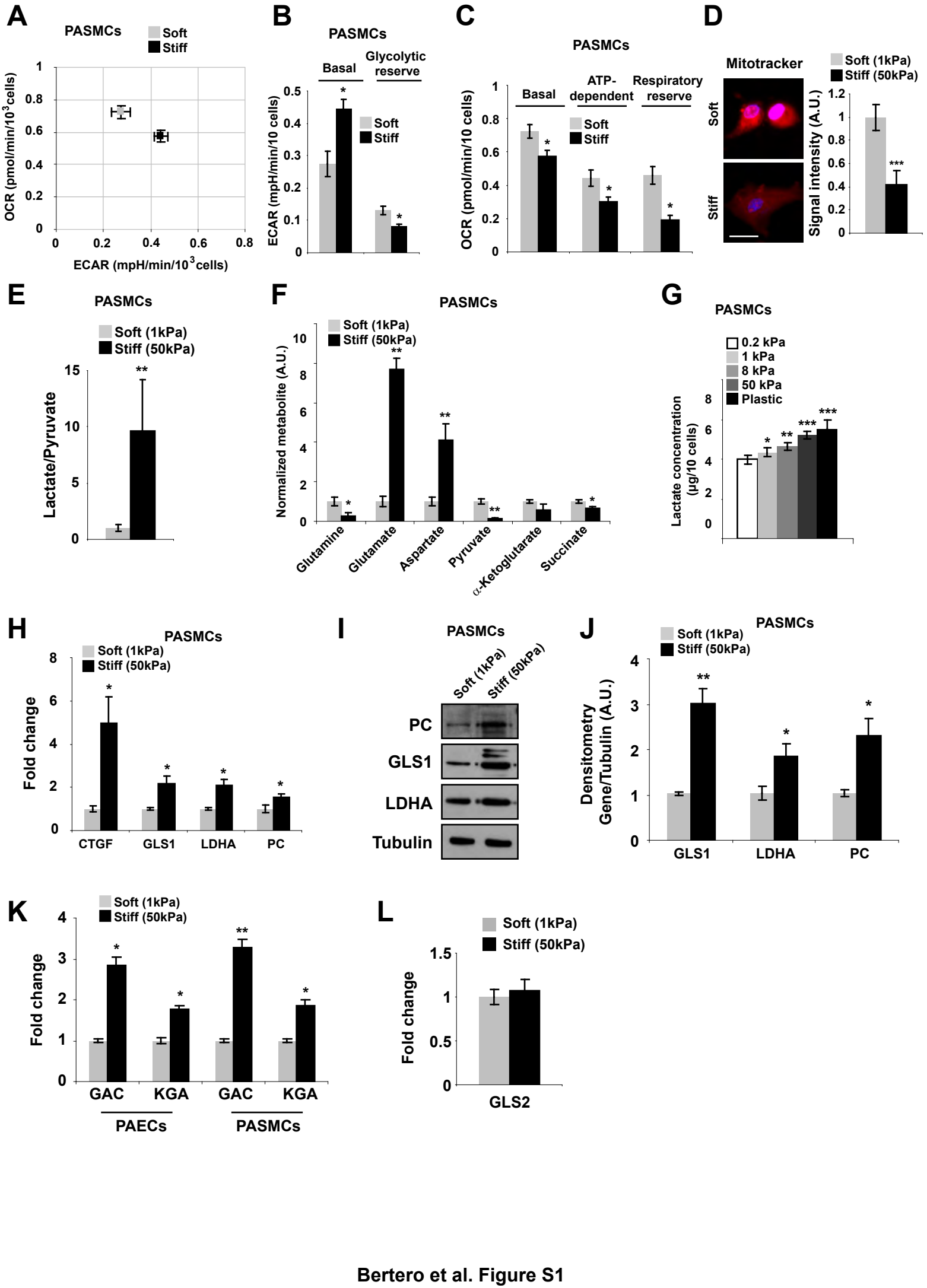

Bertero et al. Figure S1

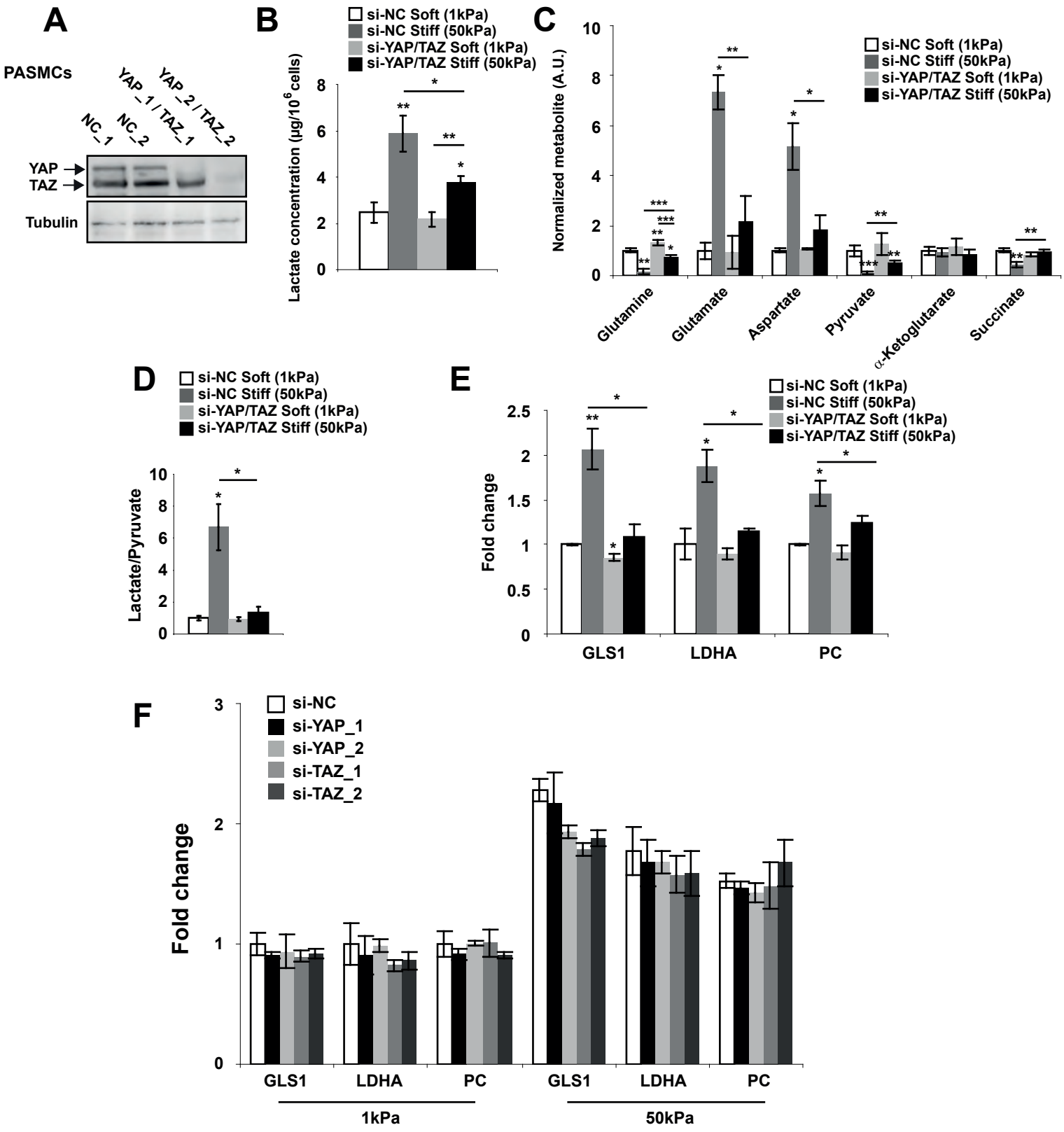

Bertero et al. Figure S2

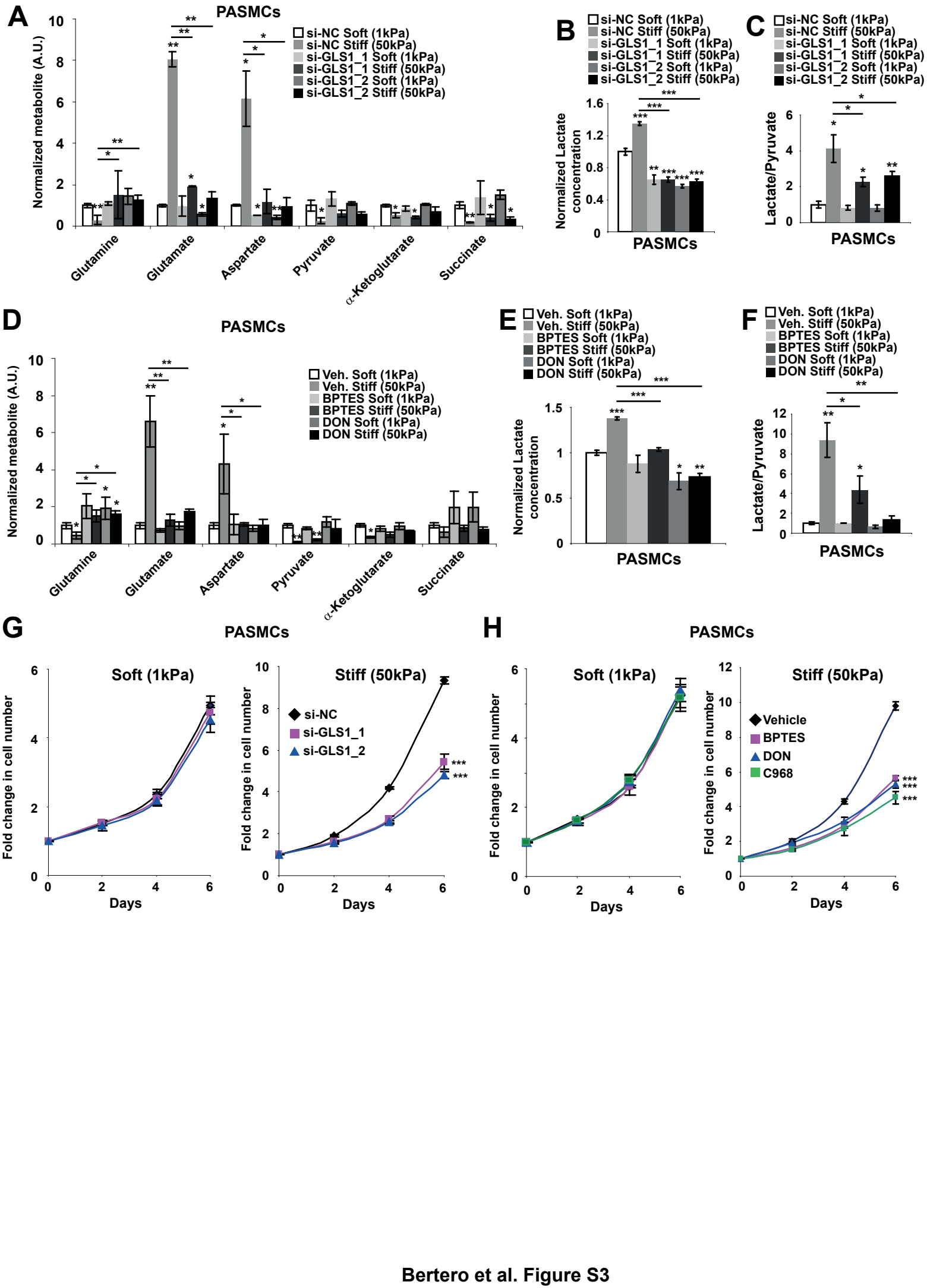

Bertero et al. Figure S3

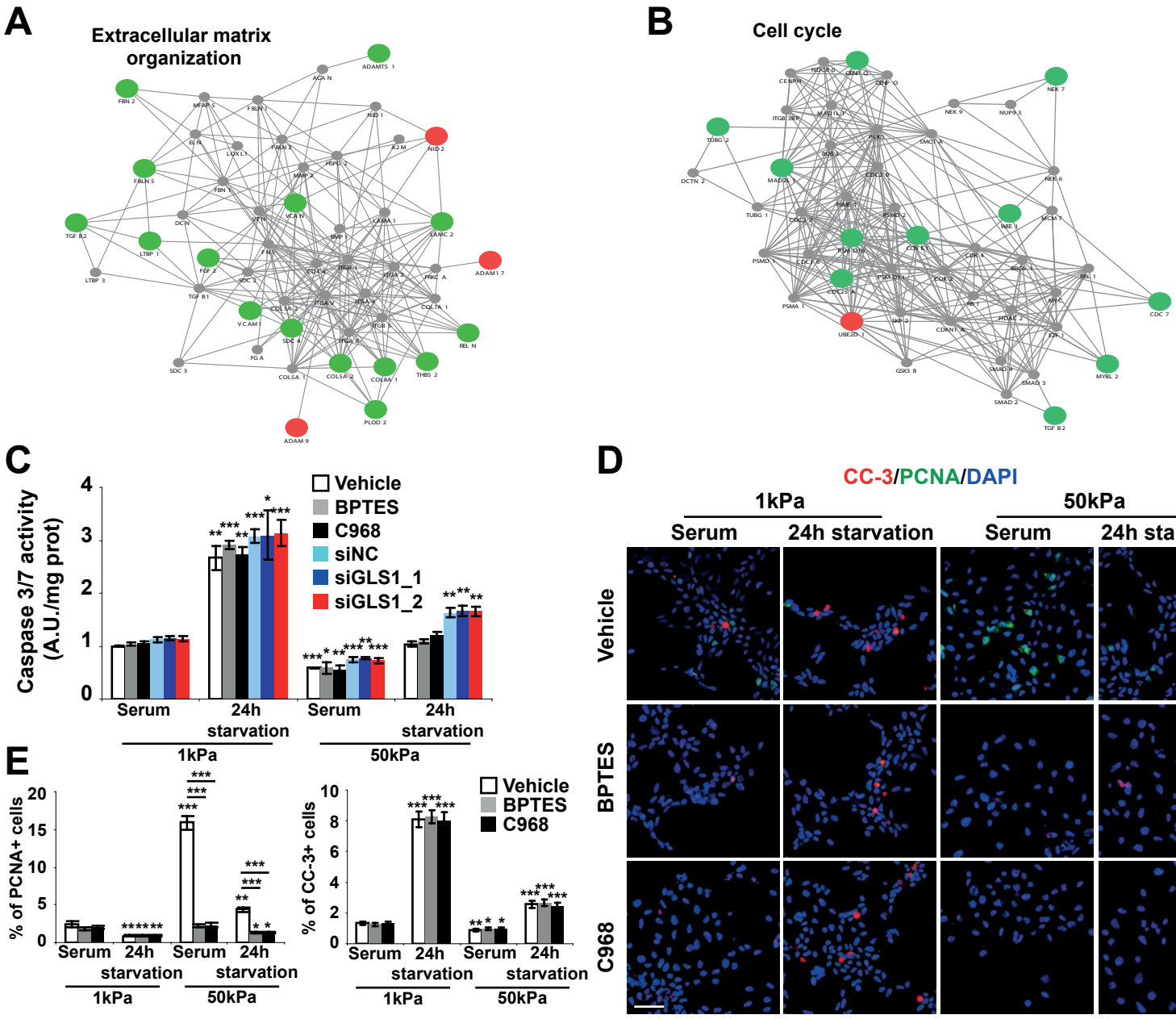

Bertero et al. Figure S4

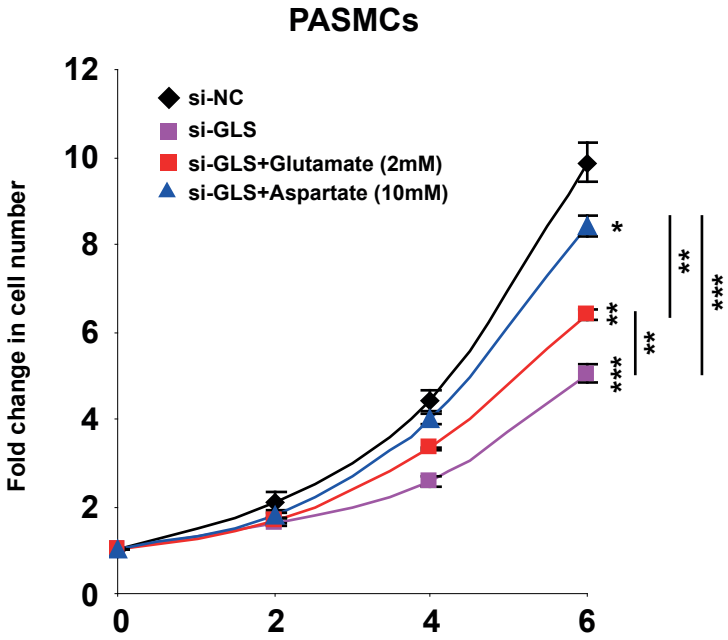

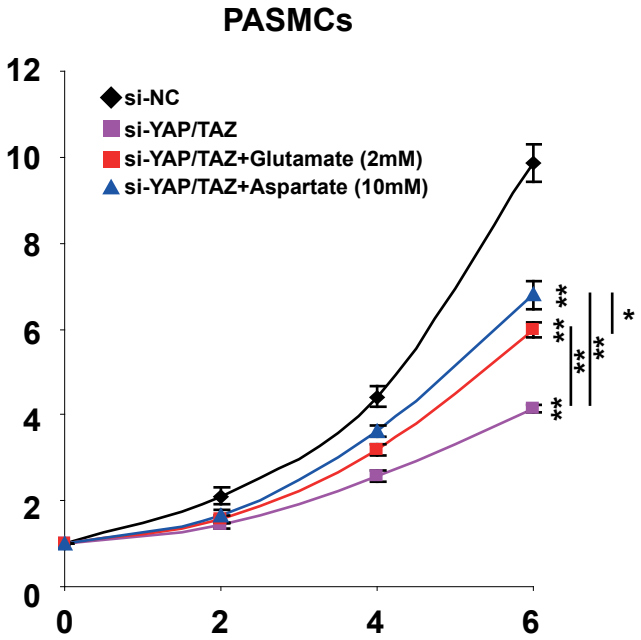

Bertero et al. Figure S5

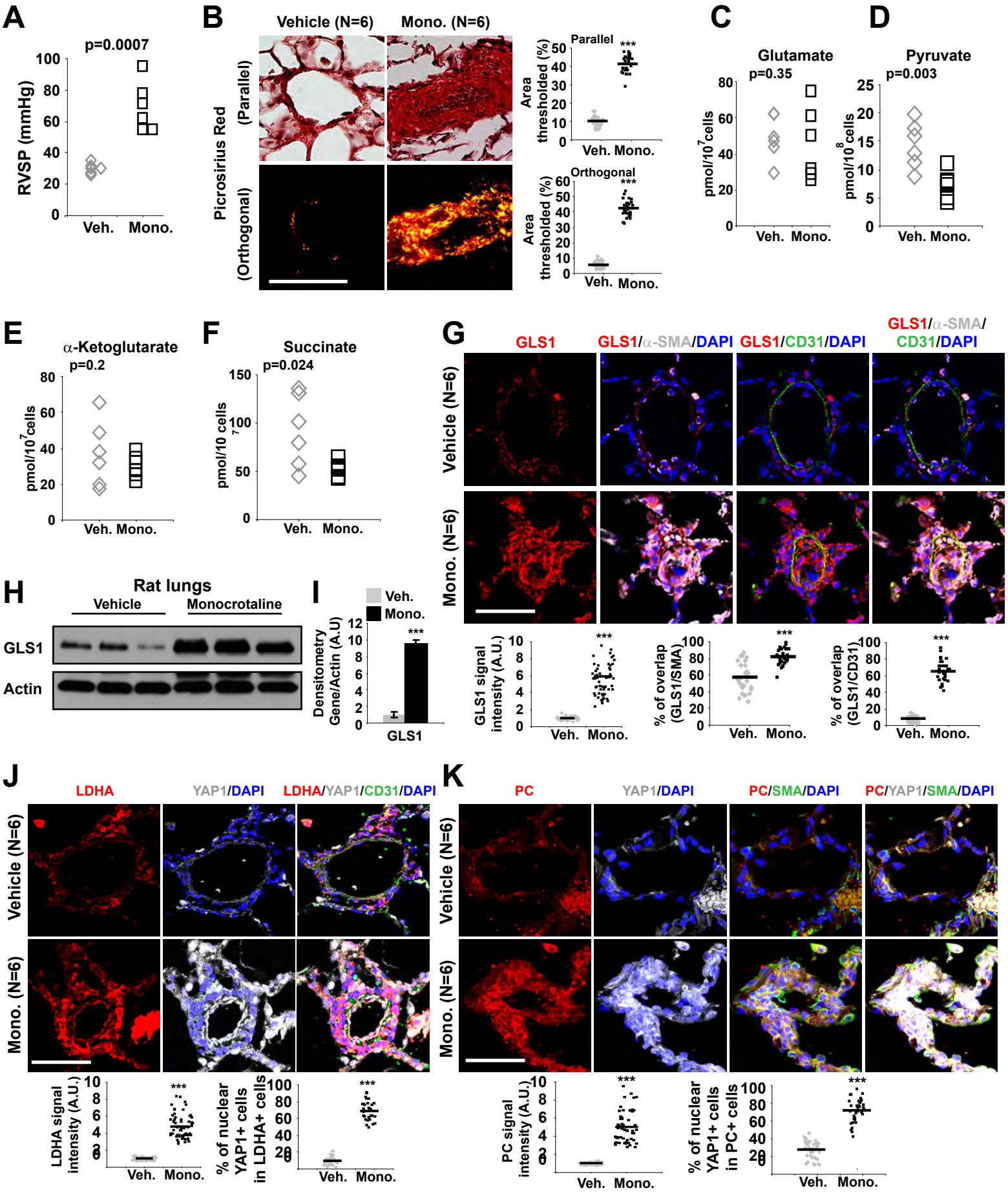

Bertero et al. Figure S6

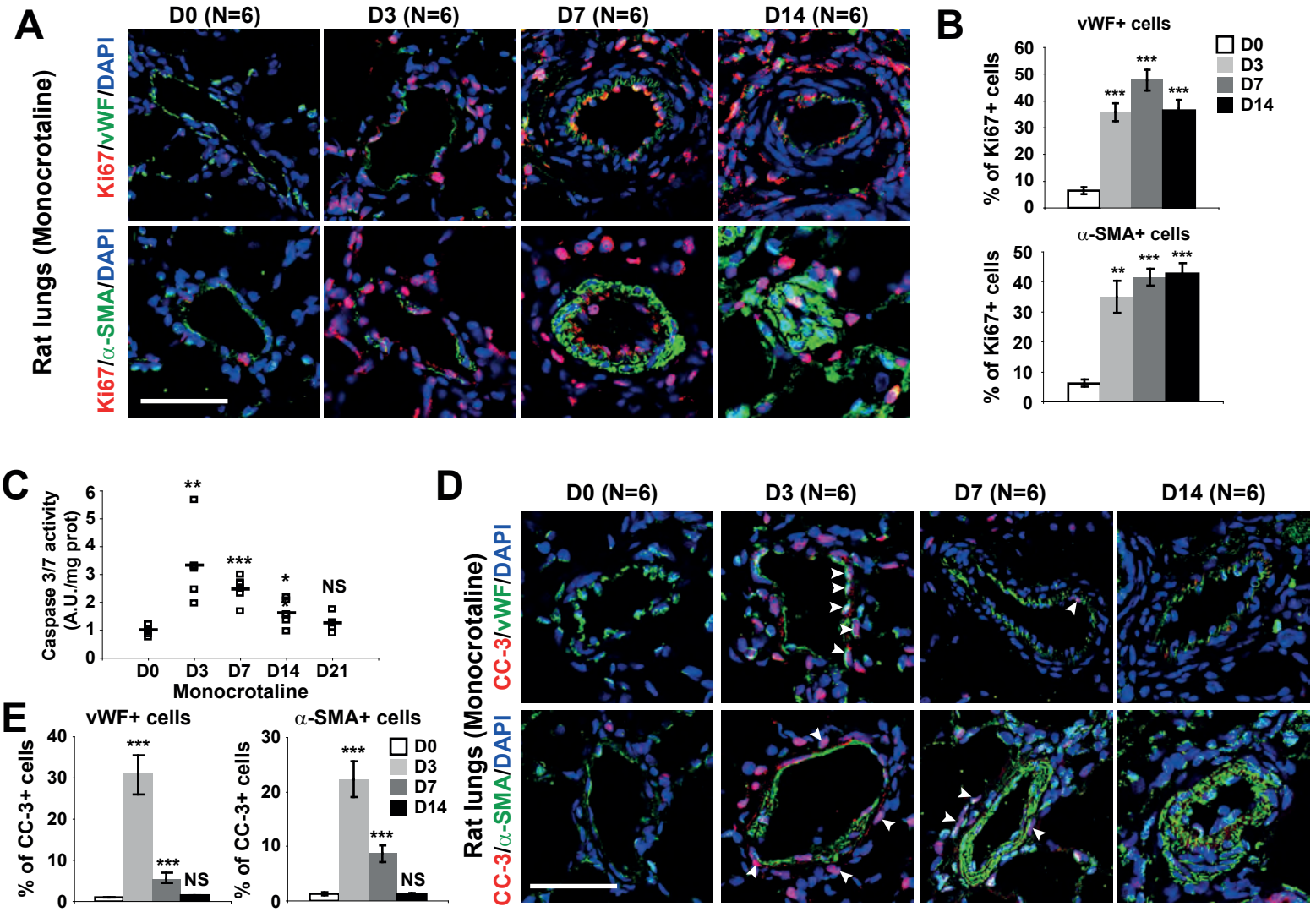

Bertero et al. Figure S7

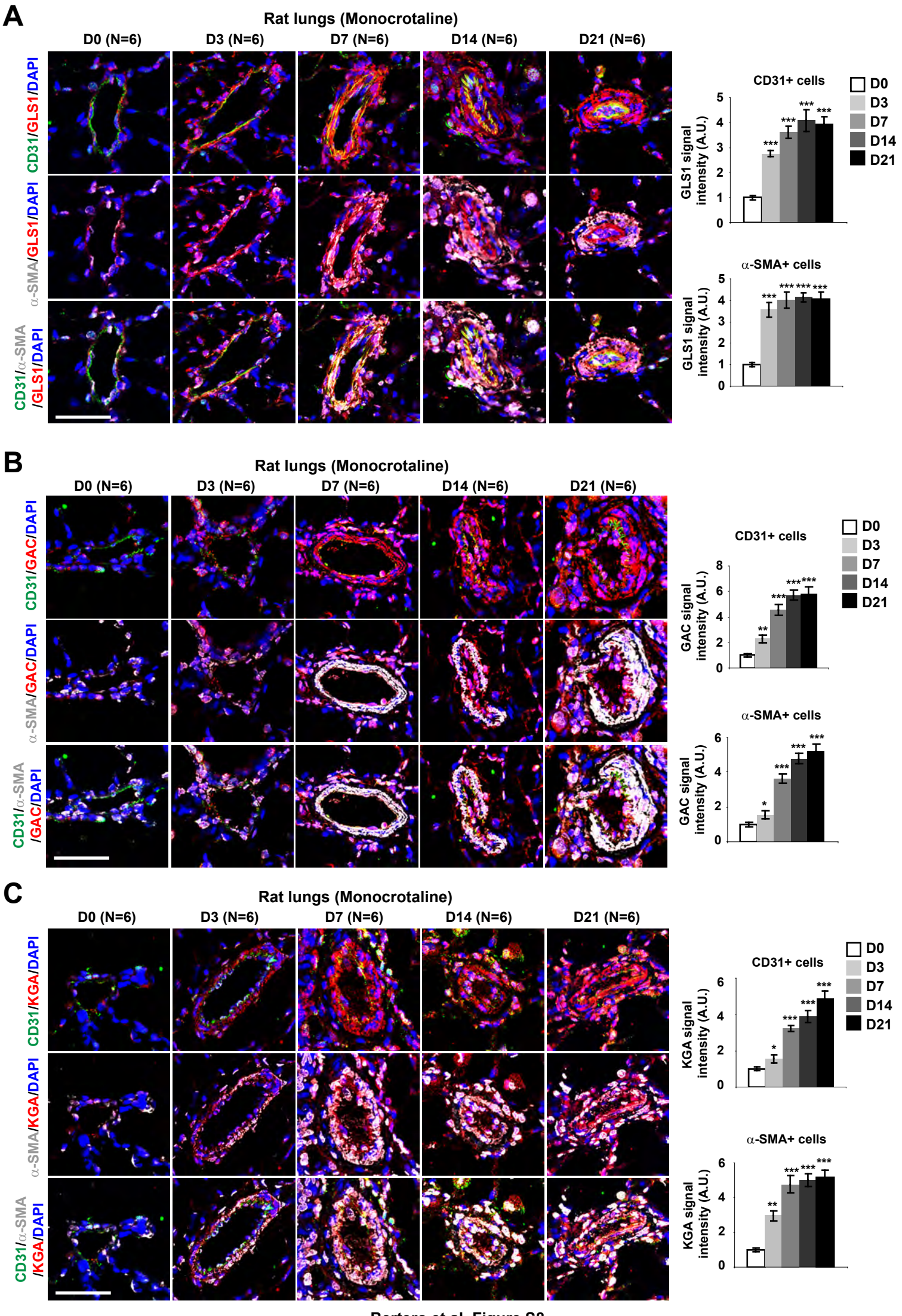

Bertero et al. Figure S8

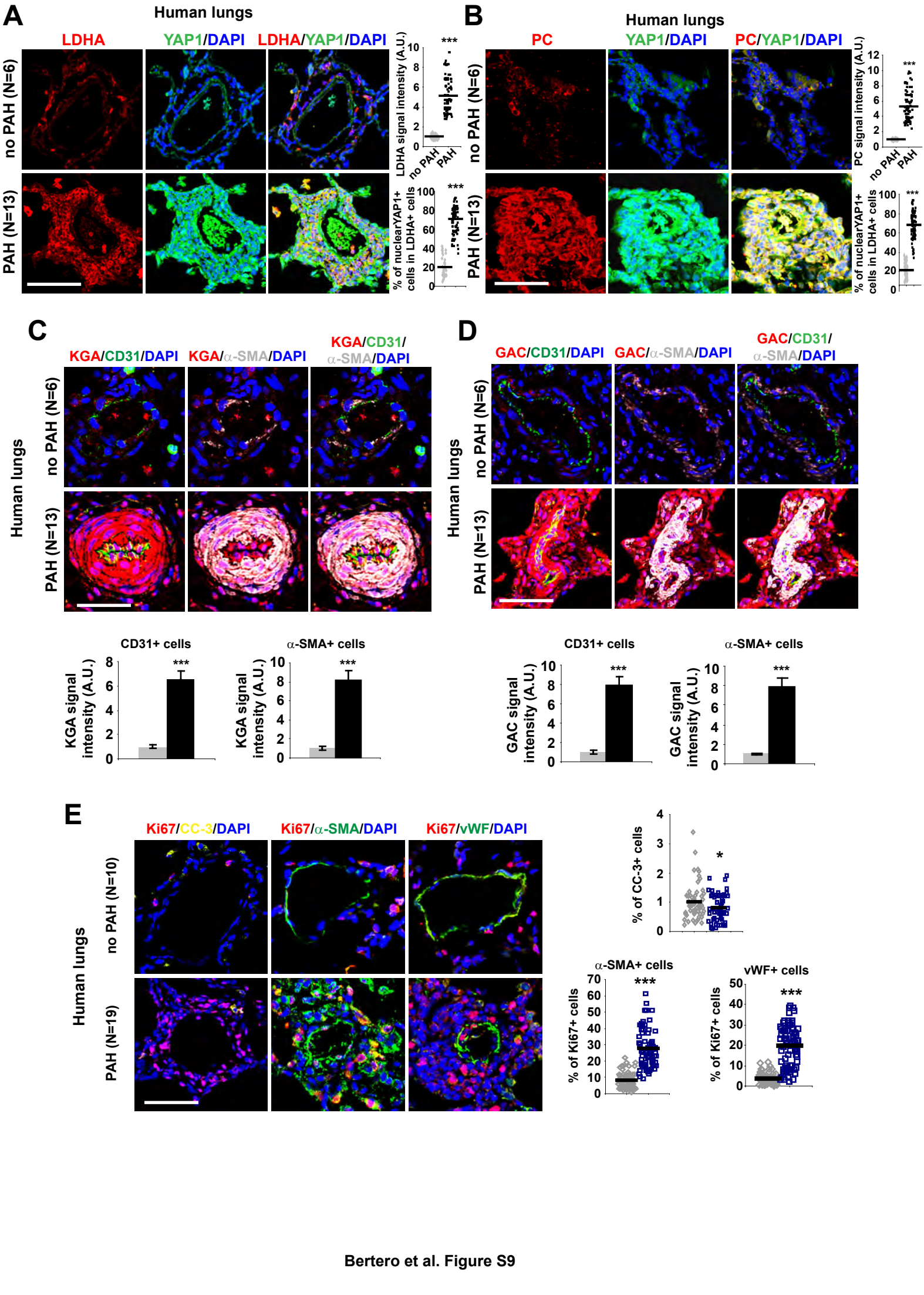

Bertero et al. Figure S9

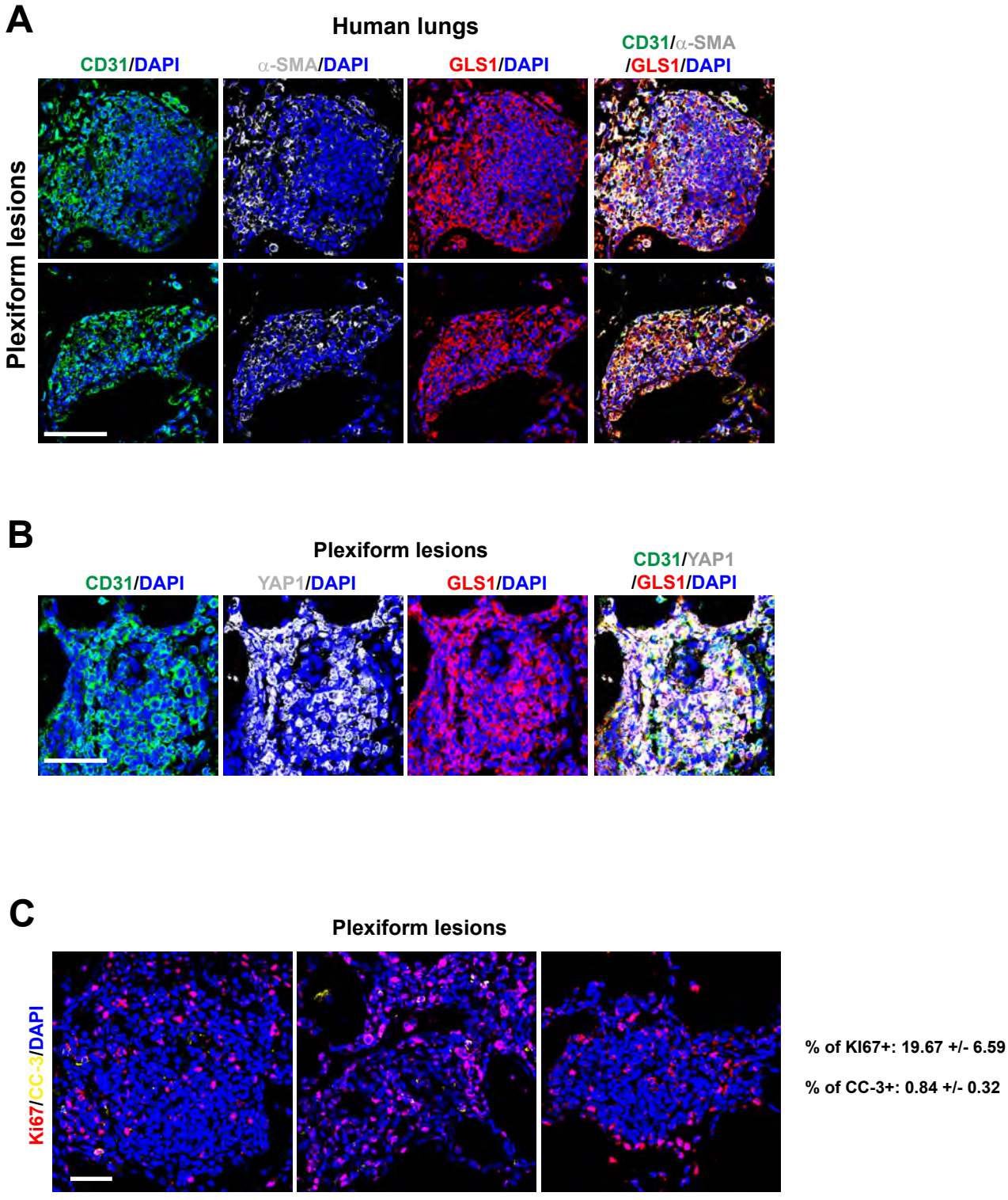

Bertero et al. Figure S10

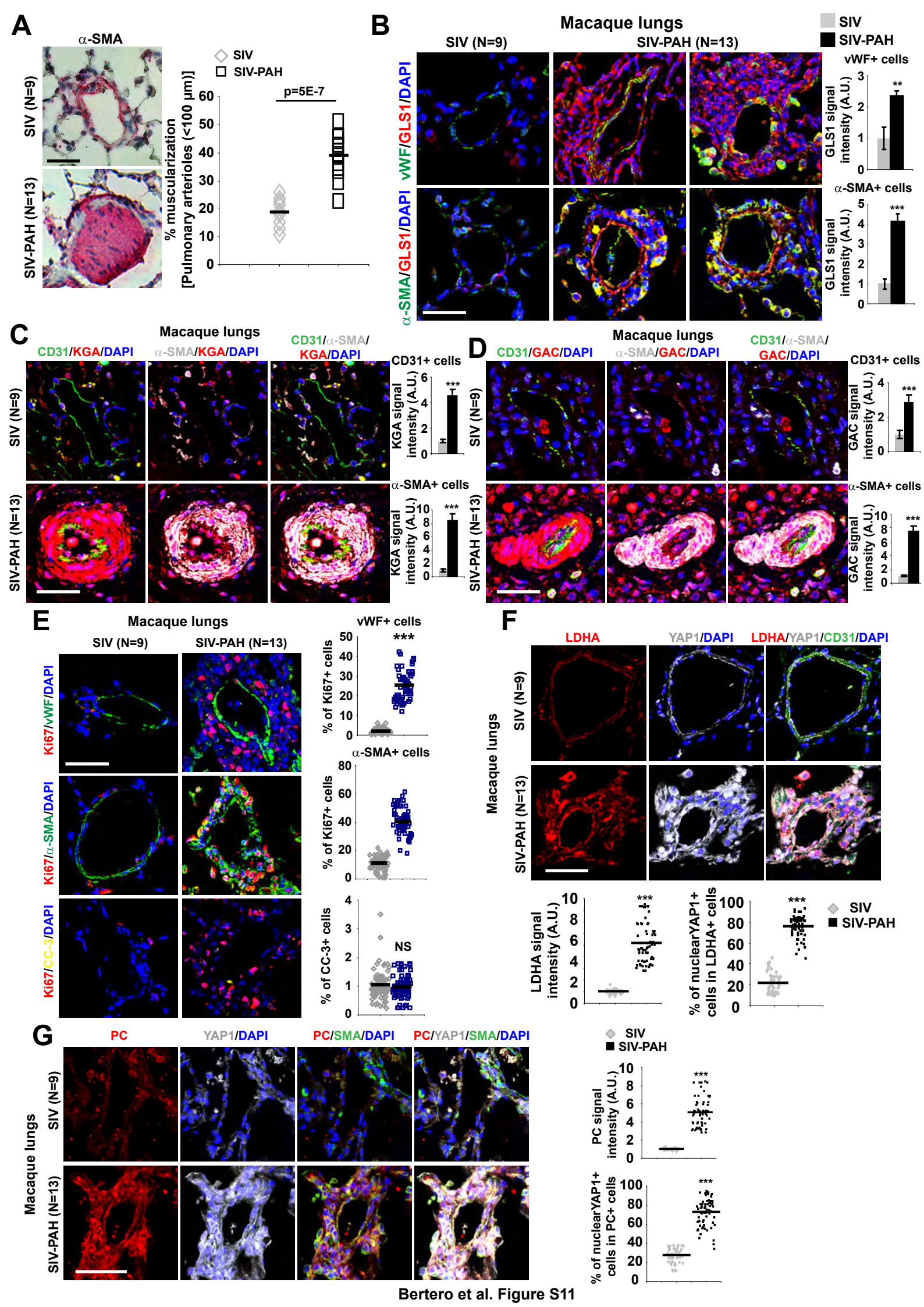

Bertero et al. Figure S11

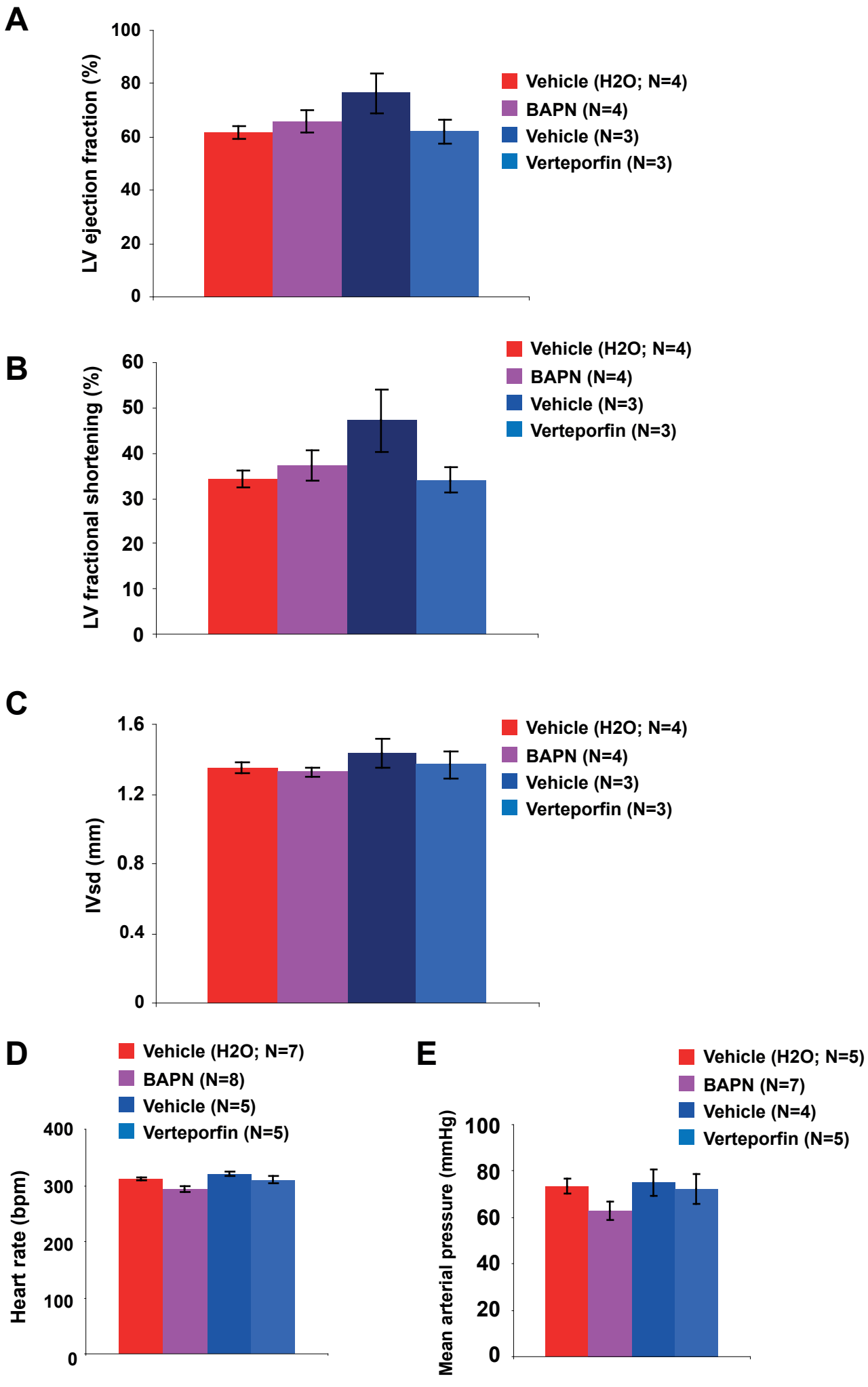

Bertero et al. Figure S12

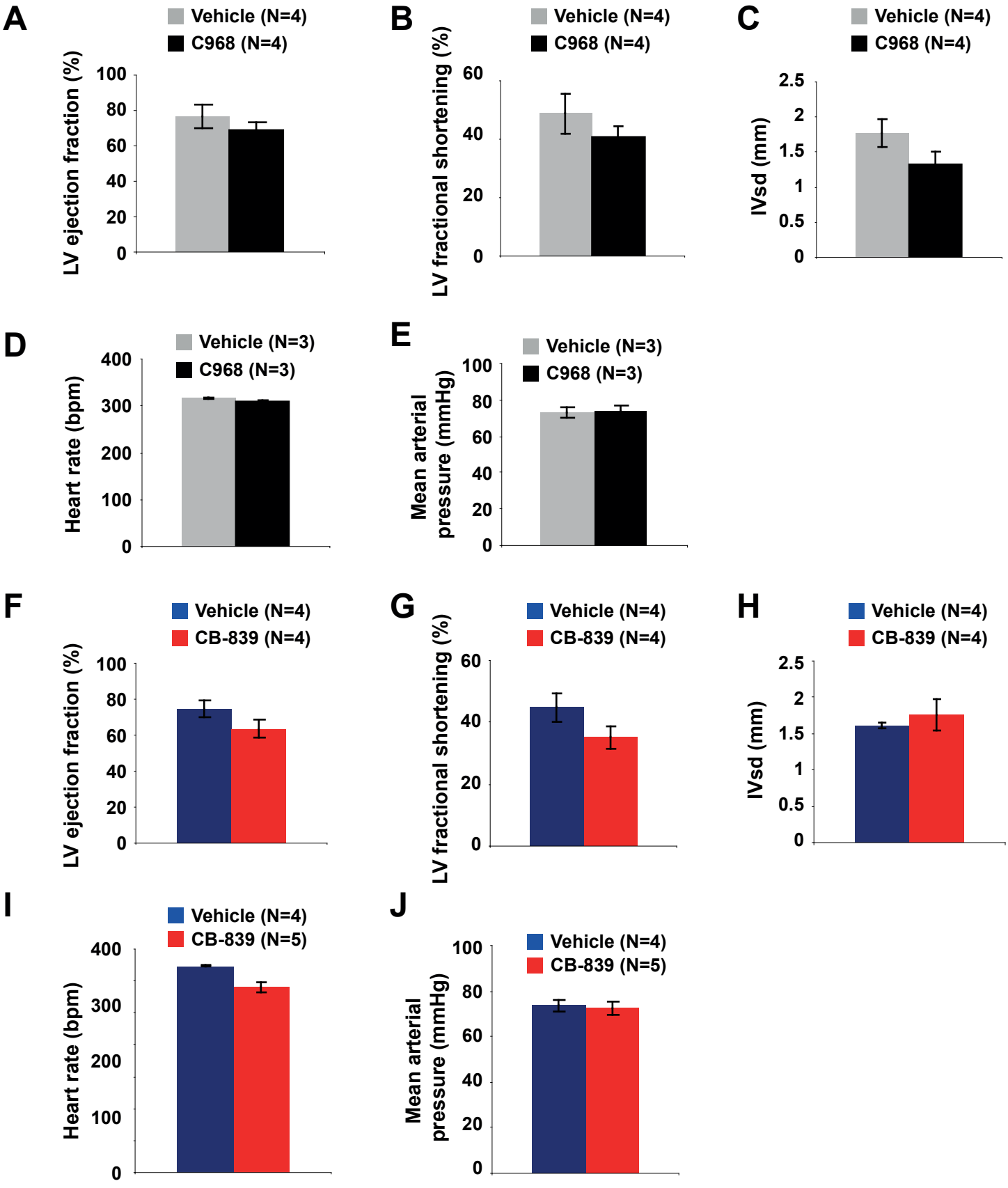

Bertero et al. Figure S13

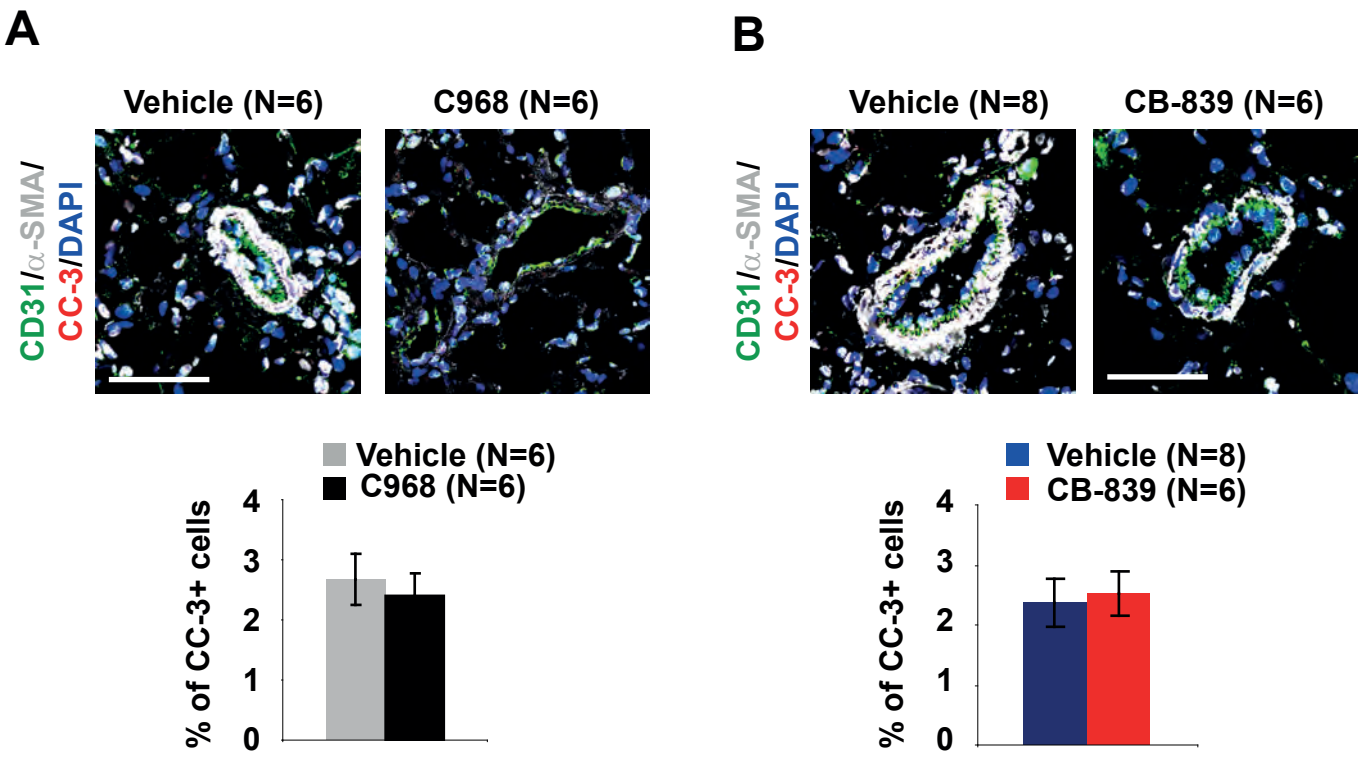

Bertero et al. Figure S14

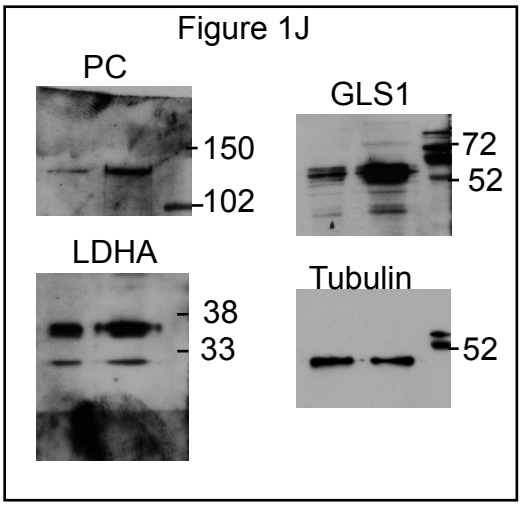
Figure 1J
PC
150
102
GLS1
72
52
LDHA
38
33
Tubulin
52

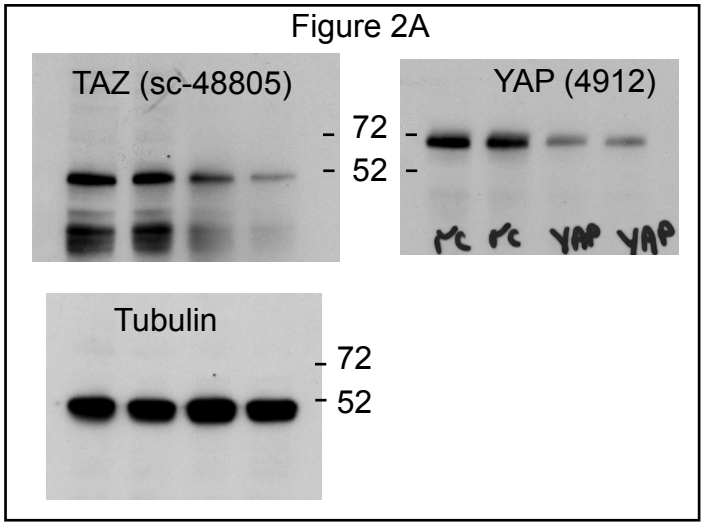
Figure 2A
TAZ (sc-48805)
72
52
YAP (4912)
Tubulin
72
52

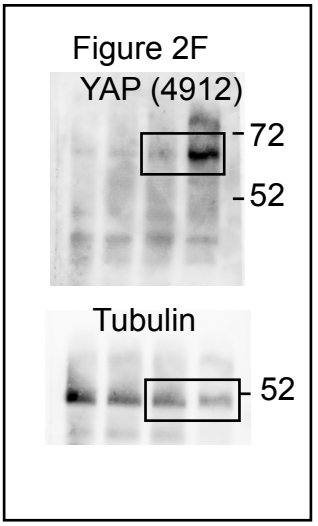
Figure 2F
YAP (4912)
72
52
Tubulin
52

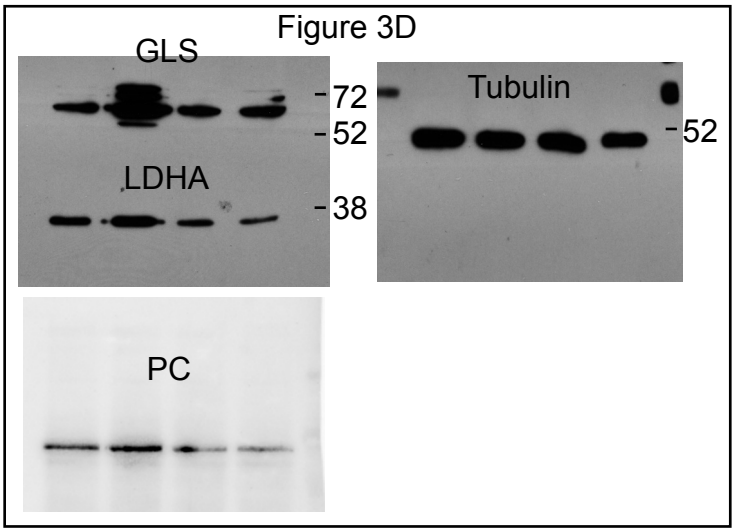
Figure 3D
GLS
72
52
LDHA
38
Tubulin
52
PC

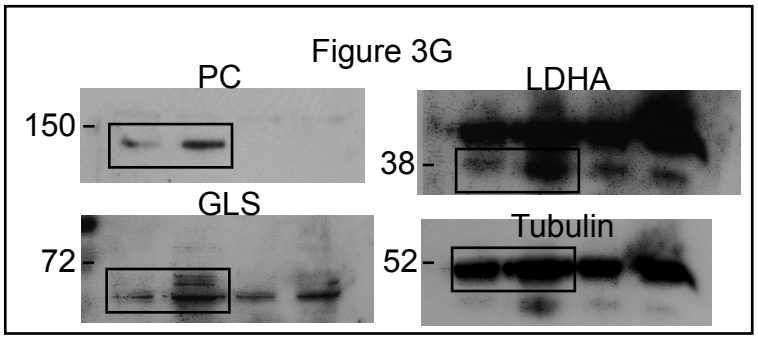
Figure 3G
PC
150
LDHA
38
GLS
72
Tubulin
52

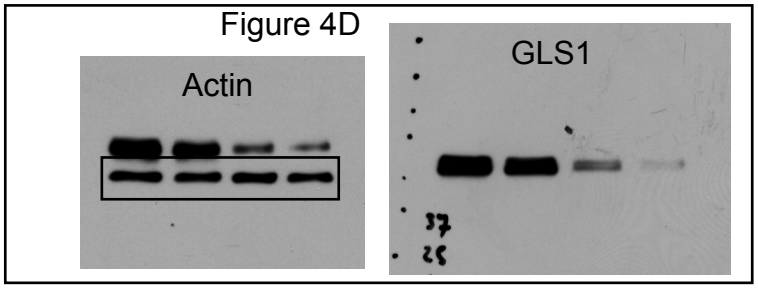
Figure 4D
Actin
GLS1

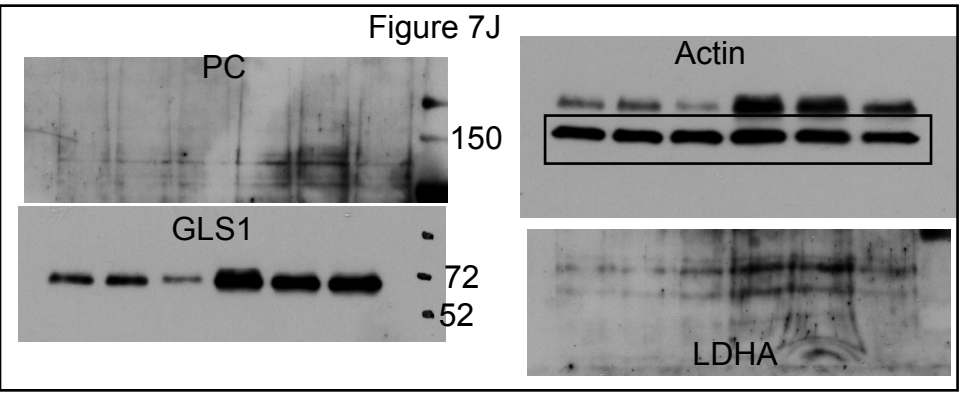
Figure 7J
PC
150
Actin
GLS1
72
52
LDHA

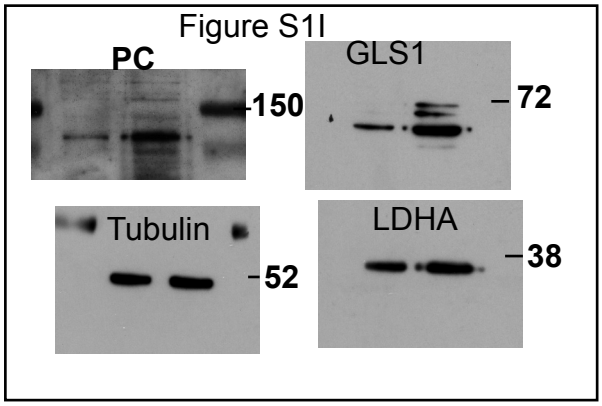
Figure S1I
PC
150
GLS1
72
Tubulin
52
LDHA
38

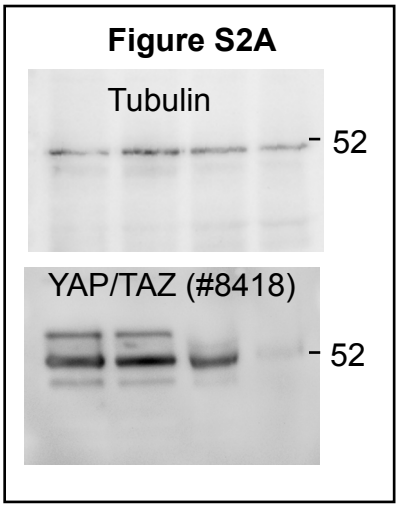
Figure S2A
Tubulin
52
YAP/TAZ (#8418)
52

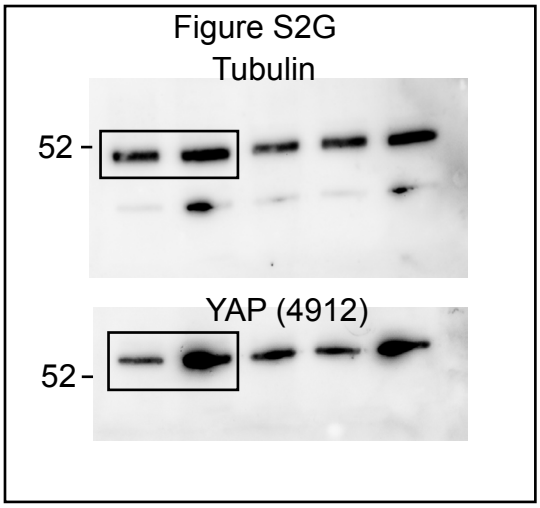
Figure S2G
Tubulin
52
YAP (4912)
52

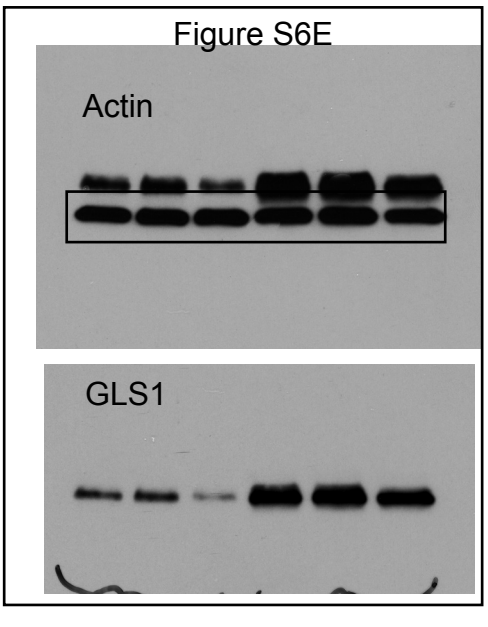
Figure S6E
Actin
GLS1